DUBLIN CITY UNIVERSITY
SCHOOL OF ELECTRONIC ENGINEERING

A Final Project report in

Simulation and exploration of THz TRNASMISSION LINES

By Mohammed AL Shuaili

BACHELOR OF ENGINEERING

IN

ELECTRONIC AND COMPUTER ENGINEERING

MAJORING IN

THE INTERNET OF THINGS

Supervised by Dr Marissa Condon

Acknowledgements

Declaration

I declare that this material, which I now submit for assessment, is entirely my own work and has not been taken from the work of others, save and to the extent that such work has been cited and acknowledged within the text of my work. I understand that plagiarism, collusion, and copying are grave and serious offences in the university and accept the penalties that would be imposed should I engage in plagiarism, collusion or copying. I have read and understood the Assignment Regulations set out in the module documentation. I have identified and included the source of all facts, ideas, opinions, and viewpoints of others in the assignment references. Direct quotations from books, journal articles, internet sources, module text, or any other source whatsoever are acknowledged and the source cited in the assignment references. This assignment, or any part of it, has not been previously submitted by me or any other person for assessment on this or any other course of study.

I have read and understood the DCU Academic Integrity and Plagiarism policy at https://www.dcu.ie/policies/academic-integrity-plagiarism-policy

Name: Mohammed Al Shuaili Date: 21/2/2025

Abstract

This final report presents the simulation and exploration of terahertz (THz) transmission lines, focusing on the development and validation of numerical models for high-frequency applications. The project addresses the challenges of accurately modelling THz transmission lines, which are essential for next-generation technologies such as 6G networks, wireless data centres, and biomedical imaging. The primary goal is to create computationally efficient and precise models capable of simulating time-domain behaviour at THz frequencies. Three key methods were employed: the Finite-Difference Time-Domain (FDTD) approach for initial approximations, the Numerical Inverse Laplace Transform (NILT) for exact s-domain solutions, and RLC ladder approximations for efficient time-domain modelling. The FDTD simulations provided a baseline for understanding transient and steady-state behaviours, while the RLC ladder method, combined with NILT, demonstrated the ability to closely match exact solutions when sufficient sections were used. Additionally, Y-parameters were derived to analyse transmission line behaviour, and Asymptotic Waveform Evaluation (AWE) was implemented to refine approximations and extract dominant system responses. The final model was obtained through iterative addition of small responses at high frequencies and comparison with exact solutions. The results highlight the importance of optimising the number of sections in the model to balance accuracy and computational efficiency. This work contributes to the advancement of THz communication systems by providing reliable modelling tools for future research and development.

Table of Contents

Table of Figures (need a fix)

Chapter 1 – Introduction

The growing demand for wireless data rates exceeding 100 Gbit/s, driven by applications such as 5G backhaul/fronthaul, data centres, and intra-device links, has spurred interest in terahertz (THz) frequencies (0.1–10 THz) [1]. This spectrum offers vast bandwidths, enabling high-speed THz communications for 6G networks and applications such as remote sensing, biomedical imaging, and space communication [2]. However, challenges such as developing accurate channel models, reliable RF components, and standardized measurement methods remain [1]. Recent hardware advancements, using both electronic and photonic approaches, demonstrate progress, but further research is essential to bridge the gap between theoretical potential and practical deployment.

This project aims to develop and validate efficient numerical models for THz transmission lines to predict signal behaviour and optimize system performance. The study addresses key propagation challenges at THz frequencies, such as high attenuation and dispersion, which are critical for the design of next-generation communication systems. To achieve this, the project evaluates original methods and techniques proposed between 2000 and 2010, assessing their suitability for THz applications. In addition, the research focuses on developing an accurate model using Y-parameters and Asymptotic Waveform Evaluation (AWE). The developed model is then compared with the original methods to determine their effectiveness and limitations at THz frequencies.

Three primary methods are used in this study: Finite-Difference Time-Domain (FDTD) for transient analysis, Numerical Inverse Laplace Transform (NILT) for obtaining the exact response from the exact s-domain solution, and RLC ladder approximation for computational efficiency. The FDTD method provides a foundation for simulating time-domain electromagnetic wave propagation, while the exact model offers precise frequency-domain insights and the NILT response serving as a benchmark for evaluating other methods. The RLC ladder approximation, on the other hand, is used to simplify complex transmission line models, making them computationally tractable for large-scale simulations. These methods are compared against each other and to the obtained model using Y-parameters and Asymptotic Waveform Evaluation (AWE) to evaluate their effectiveness for THz applications. Factors affecting their performance, such as the number of sections, computational cost, and accuracy, are analysed to determine the most efficient approach for THz transmission line modelling.

The report includes a literature review, implementation details of these modelling methods, simulation results, challenges faced, and future work plans. By integrating Y-parameters and AWE into the modelling framework, this research aims to establish a validated numerical approach for THz transmission line modelling. The proposed model addresses the limitations of earlier methods and offers the best computationally efficient and accurate solution for THz signal analysis. By comparing the developed model with original methods from 2000 to 2010, this study provides valuable insights into the evolution of THz modelling techniques and their applicability to modern communication systems. This research aims to advance THz communication technologies by designing high-performance systems capable of operating at high frequencies.

1.2 Summary

This project develops and validates numerical models for THz transmission lines to optimize system performance and address propagation challenges. Three primary methods—FDTD, NILT (exact solution), and RLC ladder approximations—are evaluated for accuracy, computational efficiency, and effectiveness compared to the obtained model using AWE. Additionally, MATLAB circuit code-based analyser is used for the implementation, but these methods can be applied using any coding language or software.

Chapter 2- Technical Background

Modelling THz (0.1–10 THz) transmission lines require understanding wave propagation, transmission line theory, and numerical methods. At THz frequencies, the behaviour of transmission lines is governed by the Telegrapher's equations (1), which describe the relationship between voltage and current along the line. These equations are derived from Maxwell's equations and are given by [3]:

$$\frac{dv(x,t)}{dx} = -R(x)\, i(x,t) - L(x)\frac{di(x,t)}{dt} \tag{1a}$$

$$\frac{di(x,t)}{dx} = -G(x)\, v(x,t) - C(x)\frac{dv(x,t)}{dt} \tag{1b}$$

where $v(x,t)$ and $i(x,t)$ represent the voltage and current at position x and time t, respectively. $R,\ L,\ G,$ and C are the per-unit-length resistance, inductance, conductance, and capacitance of the transmission line. At THz frequencies, these parameters become highly frequency-dependent, making accurate modelling more complex.

2.1 Finite-Difference Time-Domain (FDTD) Method

The FDTD method is a widely used numerical technique for solving electromagnetic problems, particularly in the time domain. It discretizes the transmission line into small segments as in Figure 1, allowing for the simulation of voltage and current over time. The FDTD method is based on approximating the derivatives in the Telegrapher's equations using finite differences [4]. In this approach voltages (v_n) are calculated at the ends of each section, while currents (i_n) are computed at the middle of each section as illustrated in Figure 1 and 2. Then, v_n and i_n can be derived as.

$$v_k^{n+1} = v_k^n - \frac{\Delta\mathrm{t}}{\Delta\mathrm{xC}}\left(i_k^{n+\frac{1}{2}} - i_{k-1}^{n+\frac{1}{2}}\right) \tag{2a}$$

$$i_{k-1}^{n+3/2} = i_k^{n+1/2} - \frac{\Delta\mathrm{t}}{\Delta\mathrm{xL}}\left(v_{k+1}^{n+1} - v_k^{n+1}\right) \tag{2b}$$

This method provides a foundation for simulating transient and steady-state behaviours of transmission lines, but it can be computationally intensive, especially for long lines or high frequencies.

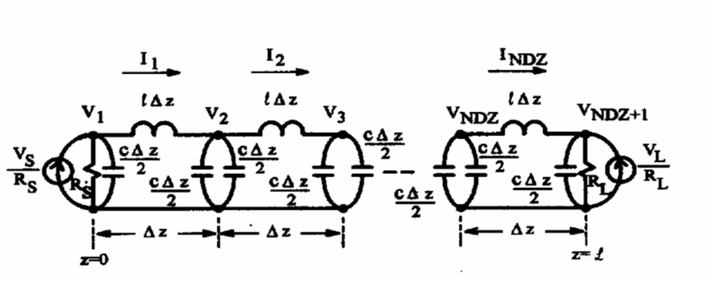

Figure 2.1: Equivalent representation of the transmission line using the Lumped Pi circuit model, illustrating the discretization of the line [4]

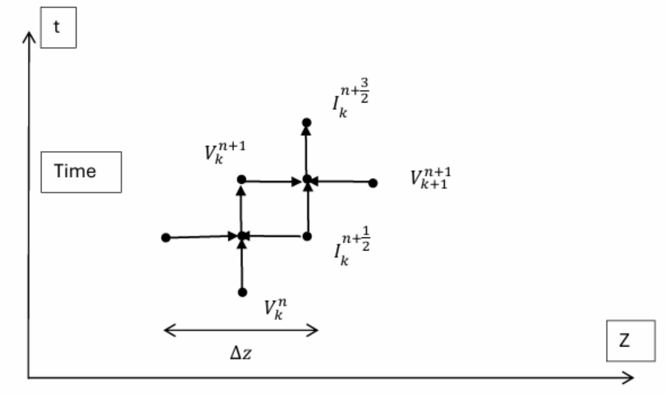

Figure 2.2: Staggered grid representation for the FDTD method, illustrating the spatial (z) and temporal (t) discretization. The voltage (V) is defined at grid points, while the current (I) is defined at the midpoints between the grid points [4]

2.2 Numerical Inverse Laplace Transform (NILT)

The NILT method is a powerful tool for converting frequency-domain solutions into time-domain solutions for simulating transient phenomena in multiconductor transmission line (MTL) systems [7]. NILT0, the baseline variant, approximates time-domain responses using residues and poles of a Padé rational function, enabling sparse time points with L-stability which damps errors exponentially for stiff systems, ensuring stability even with large time steps. L-stability as explained in equation (3) [10], prevents oscillations and guarantees accurate transient simulations with sparse sampling. NILTn (for *n*≥1) extends this by recursively computing high-order derivatives of Laplace-domain solutions, reducing truncation errors a factor of (n+1) N+M, where *n* represents the derivative order, and *N* and *M* are parameters of the Padé rational approximation that define the degrees of the numerator and denominator, respectively. Importantly, NILTn achieves this improvement while preserving numerical stability [6].

A general first-order differential equation can be expressed as:

$$\frac{dy}{dt} = \gamma y \tag{3a}$$

Applying the backward difference method to equation (4), we obtain:

$$\frac{y_n - y_{n-1}}{h} = \gamma y_n \tag{3b}$$

Rearranging the equation:

$$y_n(1 - h\gamma) = y_{n-1} \tag{3c}$$

$$\frac{y_n}{y_{n-1}} = \frac{1}{1 - h\gamma} \tag{3d}$$

For numerical stability, we consider the following conditions:

- If $\left|\frac{1}{1-h\gamma}\right| < 1$, it is an A-stable method. (3e)
- If $\left(\frac{1}{1-h\gamma}\right)^n$ → $0\ as\ n$ → ∞ the method is L-stable. (3f)

Furthermore, NILTcv is based on the Bromwich integral which is a mathematical foundation for converting Laplace-domain solutions F(s) to time-domain functions f(t). This integral is numerically evaluated using the Fast Fourier Transform (FFT) and the quotient-difference (q-d) algorithm. The algorithm computes coefficients d_n by iteratively updating quotients and differences of series terms, enabling accurate approximation with fewer terms. Thus, it transforms a slowly converging infinite series into a continued fraction which converges faster and more efficiently. The time-domain function *f*(*t*) is approximated using a discrete form derived from the Laplace transform *F*(*s*) as in (4). The approximation involves a finite sum evaluated by the FFT and an infinite sum accelerated by the q-d algorithm, which uses a continued fraction to improve convergence [7][8].

$$f(t) = \frac{1}{2\pi j}\int_{c-\infty}^{c+\infty} F(s)e^{st}ds \tag{4}$$

This approach allows for the exact solution of the transmission line's behaviour in the s-domain, which can then be compared with approximate methods such as the RLC ladder to validate accuracy.

2.3 RLC Ladder Approximations

The RLC ladder method approximates a transmission line by dividing it into multiple sections, each represented by lumped resistive (R), inductive (L), and capacitive (C) elements as shown in Figure 2.3 [3][5]. This discretization simplifies the transmission line into a network of interconnected RLC circuits, making it easier to model and simulate

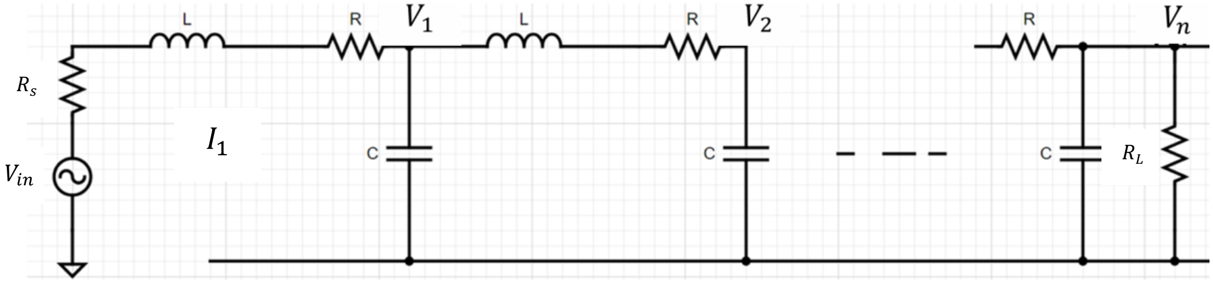

Figure 2.3: RLC ladder network approximates a transmission line with N sections and lumped elements (R), (L), and (C).

Governing equations:

Considering one section of the RLC ladder, the following equations are derived:

$$V_s - V_1 = (R + R_s)I_1\,dz + L\frac{dI_1}{dt}dz \tag{5}$$

$$I_1 - I_2 = C\frac{dV_1}{dt}dz \tag{6}$$

here, dz represents the length of a small segment of the transmission line and is defined as:

$$dz = \frac{l}{N} \tag{7}$$

where *l* is the total length of the line, and *N* is the number of sections or RLC circuits used to model the line.

$$\frac{dI_1}{dt} = -\frac{1}{L}V_1 - \frac{R_s + R}{L}I_1 + \frac{1}{L}V_s \tag{8}$$

$$\frac{dV_1}{dt} = \frac{1}{C}I_1 - \frac{1}{C}I_2 \tag{9}$$

$$\frac{dI_n}{dt} = -\frac{1}{L}V_n - \frac{R}{L}I_n + \frac{1}{L}V_{n-1} \tag{10}$$

$$\frac{dV_n}{dt} = \frac{1}{C}I_n - \frac{1}{C}I_{n+1} \tag{11}$$

The impedances *R*, *L*, and *C* are defined per unit length (i.e., per *dz*) in Equations (5) and (6). By rearranging Equations (5) and (6), Equations (8) and (9) are obtained. For the *n*-th section, the generalised forms are given by Equations (10) and (11). The accuracy of the RLC ladder approximation depends on the number of sections used; more sections generally lead to higher accuracy but at the cost of increased computational complexity. The RLC ladder method is particularly useful for simulating long transmission lines or systems with complex terminations.

2.4 Asymptotic Waveform Evaluation (AWE):

Asymptotic Waveform Evaluation (AWE) is a computationally efficient technique used to approximate the transient response of large linear systems, such as electrical interconnects, by reducing their high-order state-space models into lower-order approximations. Traditional methods such as methods in SPICE become prohibitively slow for circuits with hundreds of nodes (e.g., PEEC models), but AWE addresses this by extracting dominant poles and residues from the system's transfer function using Padé approximation and moment matching [9]. By focusing on these critical poles, AWE converts the state-space representation—which describes the system's dynamics through differential equations—into a simplified time-domain model.

2.4.1 A general definition of moments in AWE:

The q^{th} moment is defined as:

$$H(s=0)=\int_0^\infty h(t)dt \tag{12}$$

$$H^{(1)}(s=0)=-\int_0^\infty h(t)tdt$$

$$H^{(2)}(s=0)=\int_0^\infty h(t)t^2dt$$

$$H^{(3)}(s=0)=-\int_0^\infty h(t)t^3dt$$

Application of moments to represent the transfer function $H(s)$:

$$\begin{aligned} H(s) &= \int_0^\infty h(t)(1-st+\frac{1}{2}s^2t^2-\frac{1}{6}s^3t^3+\frac{1}{24}s^4t^4)dt \\ &= H(0)+sH^{(1)}(0)+\frac{1}{2}s^2H^{(2)}(0)+\frac{1}{6}s^3H^{(3)}(0)+\cdots \\ &= m_0+m_1s+m_2s^2+m_3s^3+\cdots \\ &= \sum\nolimits_{k=0}^{\infty}\frac{s^k}{k!}H^{(k)}(s=0)=\sum\nolimits_{k=0}^{\infty}m_ks^k \end{aligned} \tag{13}$$

where

$$m_k = \frac{1}{k!} H^{(k)}(s = 0) = \frac{(-1)^q}{q!} \int_0^\infty t^q h(t) dt \;\; [10] \tag{14}$$

2.5 Y-parameters:

In the analysis of transmission lines, the Y-parameters (admittance parameters) are commonly used to characterize the relationship between the currents and voltages at the input and output ports. These parameters are typically determined experimentally and can be approximated using rational functions of the complex frequency variable (s) as explained in equation (15) [10].

$$\begin{bmatrix} I_s \\ -I_R \end{bmatrix} = \begin{bmatrix} Y_{11} & Y_{12} \\ Y_{21} & Y_{22} \end{bmatrix} \begin{bmatrix} V_s \\ V_R \end{bmatrix} \tag{15}$$

Each one is approximated with a rational function as in equation (16):

$$Y_{ij} = \frac{(a_{nij} s^{n-1} + .. + a_{0ij})}{s^n + .. + b_{0ij}} \tag{16}$$

In the open-circuit condition, where the output current (I_R) is zero, the voltage transfer function ($\frac{V_R}{V_s}$) is derived as a ratio of these rational functions (17b). This transfer function is then converted into a state-space form, to facilitate further analysis. Finally, AWE is applied to the state-space model to obtain a time-domain representation, enabling the study of the system's transient and steady-state behaviour. This approach provides a systematic method for modelling and simulating the response of transmission lines.

$$\frac{V_R}{V_s} = -\frac{Y_{21}}{Y_{22}} = f\left(\frac{(a_{n21} s^{n-1} + .. + a_{021})}{s^n + .. + b_{021}}, \frac{(a_{n22} s^{n-1} + .. + a_{022})}{s^n + .. + b_{022}}\right) \tag{17a}$$

$$= -\frac{\frac{(a_{n21} s^{n-1} + .. + a_{021})}{s^n + .. + b_{021}}}{\frac{(a_{n22} s^{n-1} + .. + a_{022})}{s^n + .. + b_{022}}}$$

$$= \frac{f_{n-1} s^{n-1} + \ldots + f_0}{s^n + g_{n-1} s^{n-1} + .. + g_0} \tag{17b}$$

2.6 Summary

This section summarises methods for modelling transmission lines, governed by Telegrapher’s equations. Key approaches include the FDTD method for transient simulations via staggered discretization, Numerical Inverse Laplace Transform (NILT) variants (e.g., NILTcv using FFT) for frequency-to-time-domain conversion, and RLC ladder networks RLC ladder approximations (lumped-element networks). Furthermore, AWE simplifies high-order systems via dominant poles and Pade approximations, while Y-parameters characterize admittance relationships using rational functions. In addition, complex frequency hopping is implicitly integrated via pole-residue analysis and Bromwich contour methods to enhance stability and convergence in transient simulations [8] [11]. These methods address challenges in simulating transient and steady-state behaviours of THz lines, prioritizing trade-offs between accuracy, stability, and computational efficiency.

Chapter 3- Design of Transmission lines models

3.1.1 The exact solution of Transmission lines (RLCG approach):

The exact solution of the transmission line can be derived from the RLCG ladder in the frequency domain as follows [10][7].

Firstly, write Telegrapher equations (1) in state space form

$$\frac{d}{dx}\begin{bmatrix} v(x,t) \\ i(x,t) \end{bmatrix} = \begin{bmatrix} 0 & -R(x) \\ -G(x) & 0 \end{bmatrix}\begin{bmatrix} v(x,t) \\ i(x,t) \end{bmatrix} - \begin{bmatrix} 0 & -L(x) \\ -C(x) & 0 \end{bmatrix}\frac{d}{dt}\begin{bmatrix} v(x,t) \\ i(x,t) \end{bmatrix} \tag{18}$$

moving the representation in (18) to the Laplace domain,

$$\frac{d}{dx}\begin{bmatrix} V(x,s) \\ I(x,s) \end{bmatrix} = \begin{bmatrix} 0 & -Z(x,s) \\ -Y(x,s) & 0 \end{bmatrix}\begin{bmatrix} V(x,s) \\ I(x,s) \end{bmatrix} + \begin{bmatrix} 0 & L(x) \\ C(x) & 0 \end{bmatrix}\begin{bmatrix} V(x,0) \\ I(x,0) \end{bmatrix} \tag{19}$$

where $Z\,(x,s) \;=\; R(x) \;+\; sL(x)$, and $Y\,(x,s) \;=\; G(x) \;+\; sC\,(x)$ are series impedance. Now, let:

$$W(x,s) = \begin{bmatrix} V(x,s) \\ I(x,s) \end{bmatrix}, M = \begin{bmatrix} 0 & -Z(x,s) \\ -Y(x,s) & 0 \end{bmatrix}, and\ N = \begin{bmatrix} 0 & L(x) \\ C(x) & 0 \end{bmatrix}$$

where

$$\frac{dW(x,s)}{dx} = M\,W(x,s) + N\,W(x,0) \tag{20}$$

then, $W(l,s)$ at the end of the transmission line is equal to,

$$W(l,s) = \;\Phi\,\mathrm{W(0,s)} + \int_0^l e^{M(l-x)}NW(x,0)dx \tag{21}$$

where

$$\Phi = e^{Ml}, so\ \phi = \begin{bmatrix} \Phi_{11} & \Phi_{12} \\ \Phi_{21} & \Phi_{22} \end{bmatrix} \tag{22}$$

considering zero initial conditions $(i.e, at\ W(x,0) \;=\; 0)$ then,

$$W(l,s) = \;\Phi\,\mathrm{W(0,s)} \tag{23}$$

or

$$W(l,s) = \begin{bmatrix} V(l,s) \\ I(l,s) \end{bmatrix} = \begin{bmatrix} \Phi_{11} & \Phi_{12} \\ \Phi_{21} & \Phi_{22} \end{bmatrix}\begin{bmatrix} V(0,s) \\ I(0,s) \end{bmatrix}$$

considering open voltage transmission line (i.e, $I(l,s) \;=\; 0$) then,

$$\begin{bmatrix} V(l,s) \\ 0 \end{bmatrix} = \begin{bmatrix} \Phi_{11} & \Phi_{12} \\ \Phi_{21} & \Phi_{22} \end{bmatrix}\begin{bmatrix} V(0,s) \\ I(0,s) \end{bmatrix}$$

$$0 = \Phi_{21}V(0,s) + \Phi_{22}I(0,s)$$

$$I(0,s) = -\Phi_{22}^{-1}\Phi_{21}V(0,s)$$

$$V(l,s) = \Phi_{11}V(0,s) + \Phi_{12}\,I(0,s) \tag{24}$$

$$V(l,s) = \Phi_{11}V(0,s) - \Phi_{12}\,\Phi_{21}\,\Phi_{22}^{-1}V(0,s) \tag{25}$$

re arrange equation (25) and simplify, the following is achieved in the s domain,

$$V(l,s) = \frac{2V_s(s)e^{l\sqrt{YZ}}}{e^{(2l\sqrt{YZ})} + 1} \tag{26}$$

where $V_s(s)$ is the input in the s domain. However, if the source resistance is considered then equation (25) can be expressed as equation (27) and thus, $V(l,s)$ is equal to equation (28).

$$V(0,s) = V_s - R_sI(0,s)$$

$$V(0,s) = V_s - R_s(-\Phi_{22}^{-1}\Phi_{21}V_s\,)$$

$$V(0,s) = \frac{V_s}{1 - R_s\Phi_{21}\Phi_{22}^{-1}}$$

$$V(l,s) = \frac{V_s}{1 - R_s\Phi_{21}\Phi_{22}^{-1}}\,(\Phi_{11} - \Phi_{12}\,\Phi_{21}\,\Phi_{22}^{-1}) \tag{27}$$

$$\frac{V(l,s)}{V_s} = \frac{2e^{\left(l(YZ)^{\frac{1}{2}}\right)}(YZ)^{\frac{1}{2}}}{(YZ)^{\frac{1}{2}} - R_sY + e^{\left(2l(YZ)^{\frac{1}{2}}\right)}(YZ)^{\frac{1}{2}} + R_sYe^{\left(2l(YZ)^{\frac{1}{2}}\right)}} \tag{28}$$

Now, let,

$$x = \sqrt{YZ\,,}$$

$$V(l,s) = \frac{V_s(s)2e^{lx}}{e^{(2lx)} + 1}\ or\ (with\ R_s)\ V(l,s) = \frac{2xe^{lx}V_s}{e^{lx}\big((x + R_sY)e^{-lx} + (x + R_sY)e^{lx}\big)}$$

using the fact that,

$$cosh(x) = \frac{(e^x + e^{-x})}{2}\ and\ , \sinh(x) = \frac{-e^x + e^x}{2}$$

Then,

$$\frac{V(l,s)}{Vs(s)} = \frac{1}{\cosh\,(l\sqrt{YZ})}\ or\ (with\ R_s) = \frac{\sqrt{YZ}}{\sqrt{YZ}\cosh\big(l\sqrt{YZ}\big) + R_sYsinh\big(l\sqrt{YZ}\big)} \tag{29}$$

One then can use NILTcv as in code 5 in the appendix, to simulate this with different values of R, L, C and G, and ultimately compare the output to the approaches mentioned earlier.

3.1.2 Exact solution using (Lumped Element Model):

In this approach, the transmission line is represented as a cascade of small segments, each consisting of a series impedance (Z_{series}) and a parallel admittance ($Y_{parallel}$) as illustrated in Figure 3.1. These elements correspond to the physical properties of the transmission line [10].

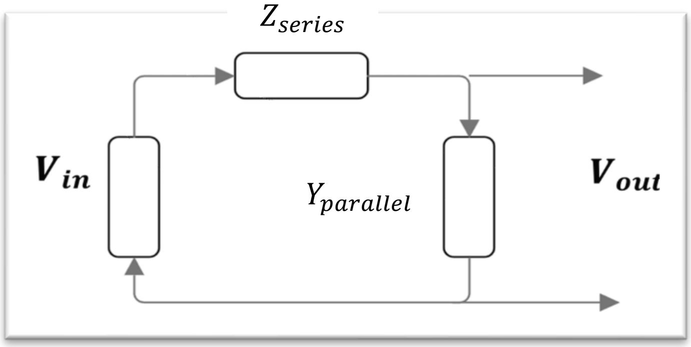

Figure 3.1: Equivalent circuit representation of a transmission line segment with series impedance (Z_series) and parallel admittance (Y_parallel).

where,

$$Z_{series} = Z_o \sinh(\gamma l)$$

$$Z_o = \sqrt{\frac{Z}{Y}}\,, \qquad Y = G + sC, \qquad Z = (R + sL), \quad \gamma = \sqrt{ZY}$$

$$Y_{parallel} = Y_o \tanh\left(\frac{\gamma l}{2}\right), \quad Y_o = \frac{1}{Z_o}\,, \quad Z_{parallel} = \frac{1}{Y_{parallel}}$$

From Figure 3.1, the following equation of the transfer function is obtained:

$$T(s) = \frac{V_o}{V_{in}} = \frac{Z_{parallel}}{Z_{series} + Z_{parallel}} \tag{30}$$

$$T(s) = \frac{V_o}{V_{in}} = \frac{\dfrac{\sqrt{\dfrac{R+sC}{G+sC}}}{\tanh\left(l\dfrac{\sqrt{(R+sC)(G+sC)}}{2}\right)}}{\sqrt{\dfrac{R+sC}{G+sC}}\sinh\left(l\sqrt{(R+sC)(G+sC)}\,\right) + \dfrac{\sqrt{\dfrac{R+sC}{G+sC}}}{\tanh\left(l\dfrac{\sqrt{(R+sC)(G+sC)}}{2}\right)}}$$

$$T(s)=\frac{V_o}{V_{in}}=\frac{\dfrac{1}{\tanh\left(l\dfrac{\sqrt{(R+sC)(G+sC)}}{2}\right)}}{\sinh\left(l\sqrt{(R+sC)(G+sC)}\right)+\dfrac{1}{\tanh\left(l\dfrac{\sqrt{(R+sC)(G+sC)}}{2}\right)}}$$

using the fact that,

$$\tanh\left(\frac{x}{2}\right)=\frac{\cosh(x)-1}{\sinh(x)}$$

$$T(s)=\frac{V_o}{V_{in}}=\frac{1}{\cosh\left(l\sqrt{(R+sC)(G+sC)}\right)} \tag{31}$$

which is the same as in equation (29).

3.2 AWE implementation:

AWE involves 4 main steps that gives the impulse response in the form of equation (32):

$$h(t)=k_0\delta(t)+k_1e^{p_1t}+\ldots+k_ne^{p_nt} \tag{32}$$

3.2.1 Step 1: Form a state – space representation out of a model (RLC ladder or general TF):

Consider 2 sections of the RLC ladder in Figure 2.3, the following equations are derived:

$$v_{in}=(R_s+R_{dz})i_1+L_{dz}\frac{di_1}{dt}+v_1 \tag{33}$$

$$v_1=R_{dz}i_2+L_{dz}\frac{di_2}{dt}+v_{out}$$

$$i_1-i_2=C\frac{dv_1}{dt}$$

$$i_2=C\frac{dv_o}{dt}$$

Let,

$$x=\begin{bmatrix}x_1\\x_2\\x_3\\x_4\end{bmatrix}=\begin{bmatrix}i_1\\v_1\\i_2\\v_o\end{bmatrix} \tag{34}$$

Rewriting the equations,

$$\frac{di_1}{dt}=-\frac{(R_s+R_{dz})}{L_{dz}}i_1-\frac{v_1}{L_{dz}}+\frac{v_{in}}{L_{dz}}$$

$$\frac{di_2}{dt} = \frac{-R_{dz} i_2}{L_{dz}} - \frac{v_{out}}{L_{dz}} + v_1$$

$$\frac{dv_1}{dt} = \frac{1}{C}(i_1 - i_2)$$

$$\frac{dv_o}{dt} = \frac{1}{C}\ i_2$$

Then the state space representation is:

$$A = \begin{bmatrix} \frac{-R_s + R_{dz}}{L_{dz}} & -\frac{1}{L_{dz}} & 0 & 0 \\ \frac{1}{C} & 0 & -\frac{1}{C} & 0 \\ 0 & \frac{1}{L_{dz}} & -\frac{R_{dz}}{L_{dz}} & -\frac{1}{L_{dz}} \\ 0 & 0 & \frac{1}{C} & 0 \end{bmatrix}, B = \begin{bmatrix} \frac{1}{L_{dz}} \\ 0 \\ 0 \\ 0 \end{bmatrix}, \quad C = [0 \quad 0 \quad 0 \quad 1]\ and\ D = 0 \tag{35}$$

In general, the RLC ladder can be expressed in state space form following the same pattern. This is coded in code 4 in the appendix, where it generates matrix A, B and C based on n number of sections.

Generally, the matrix definitions (for n stages):

1. State matrix A (size 2n x 2n)
   - Inductor rows (odd indices 1, 3, ….., 2n-1)

$$A[k,k] = -\frac{R_s+R_{dz}}{L_{dz}}, (first\ \ inductor), A[k,k] = \ -\frac{R_{dz}}{L_{dz}}\ (subsequent). \tag{36}$$

$$A[k,k+1] = \ -\frac{1}{L_{dz}}, \qquad A[k,k-1] = \frac{1}{L_{dz}}\ \ (if\ k > 1). \tag{37}$$

   - Capacitor rows (even indices 2, 4, ….., 2n).

$$A[k,k-1] = \frac{1}{C}\ , A[k,k+1] = -\frac{1}{C} \qquad (if\ k < 2n). \tag{38}$$

2. Input matrix B (size 2n x 1).

$$B = \left[\frac{1}{L_{dz}}, 0, 0, \dots\dots, 0\right]^T. \tag{39}$$

3. Output matrix C (size 1 x 2n):

$$C = [0,0,\dots\dots,0,1]. \tag{40}$$

Now, considering a general form of a transfer function that is:

$$H(s) = \frac{V_o}{V_i} = \frac{(a_{n-1}s^{n-1} + a_{n-2}s^{n-2} + \cdots + a_0)}{(s^n + b_{n-1}s^{n-1} + b_{n-2}s^{n-2} \ldots + b_0)} \tag{41}$$

Equation (41) can then be converted into a state space form as follows [11]:

$$\frac{Z(s)}{V_i} \; and \, \frac{V_o}{Z(s)}$$

$$\begin{tikzcd}
\boxed{\frac{1}{s^n + b_{n-1}s^{n-1} + .. + b_0}} \arrow[r, "Z(s)"] & \boxed{a_{n-1}s^{n-1} + a_{n-2}s^{n-2} \ldots + a_0}
\end{tikzcd} \tag{42}$$

Then, moving equation (42) to the time domain gives:

$$\frac{d^n z}{dt^n} + b_{n-1}\frac{d^{n-1}Z}{dt^{n-1}} \ldots \ldots . + b_0 Z = V_i$$

and,

$$a_{n-1}\frac{d^{n-1}Z}{dt^{n-1}} + \cdots .. + a_0 Z = V_o$$

Now, let

$$x_1 = Z \,, x_2 = \frac{dZ}{dt}, x_3 = \frac{d^2Z}{dt^2}, \ldots .., x_{n+1} = \frac{d^nZ}{dt^n} \tag{43}$$

That gives the A matrix as:

$$A = \begin{bmatrix} 0 & 1 & \ldots . & 0 & 0 \\ 0 & 0 & 1 & .. & 0 \\ .. & .. & .. & .. & 1 \\ -b_0 & -b_1 & -b_2 & \ldots .. & -b_{n-1} \end{bmatrix} \tag{44}$$

The B matrix:

$$B = \begin{bmatrix} 0 \\ 0 \\ \ldots \\ 1 \end{bmatrix}, (nx1) entries \tag{45}$$

and the C matrix: (46)

$$C = [a_0 \quad a_1 \quad \ldots .. \quad a_{n-1}]$$

One can make the rational fraction in (41) proper (numerator degree < denominator degree) by preforming polynomial division as follows.

$$H(s) = \frac{N(s)}{D(s)}$$

where,

$$N(s) = Q(s)D(s) + R(s)$$

Then the proper form is:

$$H(s) = Q(s) + \frac{R(s)}{D(s)} \tag{47}$$

where $deg(R) \ < \ deg(D)$, and the D matrix in the state space equal to $Q(s)$.

3.2.2 Step 2: Compute the moments associated with the system:

Looking at the general form of Y(s):

$$sX(s) = AX(s) + BU(s) \tag{48}$$

$$Y(s) = C^T X(s)$$

For impulse input, U(s) = 1.

$$Y(s) = C^T(sI - A)^{-1}B \tag{49}$$

If equation (49) is expanded about $s = 0$.

$$Y(s) = C^T(-A)^{-1}B - C^T(-A)^{-2}B(s) + C^T(-A)^{-3}Bs^2 \ldots$$

However, since:

$$Y(s) = m_0 + m_1 s + m_2 s^2 + .. + m_n s^n \tag{50}$$

Thus,

$$m_0 = -C(A)^{-1}B$$

$$m_1 = Y'(s_0) = -C^T(A)^{-2}B$$

$$m_2 = \frac{Y''(s_0)}{2!} = -C^T(A)^{-3}B$$

$$m_k = \frac{Y^{(k)}(s_0)}{k!} = -C^T(A)^{-(k+1)}B \tag{51}$$

However, if $s = s_0$, then expanding (49)

$$Y(s) = C^T(s_0 I - A)^{-1}B - C^T(s_0 I - A)^{-2}B(s - s_0). + \cdots$$

Thus,

$$m_0 = C(s_0 I - A)^{-1}B$$

$$m_1 = Y'(s_0) = -C^T(s_0 I - A)^{-2}B$$

$$m_2 = \frac{Y''(s_0)}{2!} = C^T(s_0I - A)^{-3}B$$

$$m_k = \frac{Y^{(k)}(s_0)}{k!} = (-1)^k C^T(s_0I - A)^{-(k+1)}B \tag{52}$$

3.2.3 Step 3: Calculate the poles of the system

In AWE, the poles and residues are determined using the system's moments in order to obtain the time-domain model as outlined in the following equations and derivations [10][9].

Consider a general form of a transfer function.

$$H(s) = \frac{a_0 + a_1s + a_2s^2 + a_3s^3}{1 + b_1s + b_2s^2 + b_3s^3 + b_4s^4} \tag{53}$$

This can be equated to: $H(s) = m_0 + m_1s + m_2s^2 + m_3s^3 + \cdots$ and,

$$(1 + b_1s + b_2s^2 + b_3s^3 + b_4s^4)(m_0 + m_1s + m_2s^2 + m_3s^3 + \cdots) \tag{54}$$
$$= a_0 + a_1s + a_2s^2 + a_3s^3$$

Multiply and equate powers of s in (54) to obtain,

$$s^0: a_0 = m_0$$
$$s^1: a_1 = m_0b_1 + m_1$$
$$s^2: a_2 = m_0b_2 + m_1b_1 + m_2$$
$$s^3: a_3 = m_0b_3 + m_1b_2 + m_2b_1 + m_3$$

Higher powers of s:

$$s^4: 0 = m_0b_4 + m_1b_3 + m_2b_2 + m_3b_1 + m_4$$
$$s^5: 0 = m_1b_4 + m_2b_3 + m_3b_2 + m_4b_1 + m_5$$
$$s^6: 0 = m_2b_4 + m_3b_3 + m_4b_2 + m_5b_1 + m_6$$
$$s^7: 0 = m_3b_4 + m_4b_3 + m_5b_2 + m_6b_1 + m_7$$

Putting this in matrix form to solve for b_i coefficients in general.

$$\begin{bmatrix} m_0 & m_1 & \ldots. & m_{q-1} \\ m_1 & m_2 & \ldots. & m_q \\ m_3 & m_4 & \ldots & .. \\ .. & \ldots & \ldots. & .. \\ m_{q-1} & \ldots & \ldots & m_{2q-1} \end{bmatrix} \begin{bmatrix} b_q \\ b_{q-1} \\ b_{q-2} \\ .. \\ b_1 \end{bmatrix} = -\begin{bmatrix} m_q \\ m_{q+1} \\ m_{q+2} \\ \ldots \\ m_{2q-1} \end{bmatrix}$$

Gaussian elimination is applied to determine the coefficients ($b_1, b_2\ , b_3, \ldots, b_q$) with ($q = 4$) in this case. The poles of the system are found by solving ($B(s)\ =\ 0$). That is, solve:

$$b_q s^q + b_{q-1} s^{q-1} \ldots\ldots + b_1 s + 1 = 0 \tag{55}$$

which gives the poles of the system.

3.2.4 Step 4: find the residues:

Generalised approach to determining the residues:

$$h(t) = \sum_{j=1}^{q} k_j e^{p_j t} \tag{56}$$

in the s domain:

$$H(s) = \sum_{j=1}^{q} \frac{k_j}{s - p_j} = \frac{a_0 + a_1 s + a_2 s^2 + \cdots + a_{q-1} s^{q-1}}{1 + b_1 s + b_2 s^2 + b_3 s^3 + \cdots + b_q s^q}$$

$$\frac{k_j}{s - p_j} = k_j \left(\frac{1}{s - p_j}\right) = -\frac{k_j}{p_j}\left(\frac{1}{1 - \frac{s}{p_j}}\right)$$

Let: $x = \frac{s}{p_j}$, Thus

$$\left(1 - \frac{s}{p_j}\right)^{-1} = 1 + \left(\frac{s}{p_j}\right) + \left(\frac{s}{p_j}\right)^2 + \left(\frac{s}{p_j}\right)^3 + \cdots \tag{57}$$

Hence,

$$H(s) = \sum_{j=1}^{q} -\frac{k_j}{p_j}\left(1 + \left(\frac{s}{p_j}\right) + \left(\frac{s}{p_j}\right)^2 + \left(\frac{s}{p_j}\right)^3 + \cdots\right) \tag{58}$$

since $H(s)$ is as in equation (50), hence

$$m_0 = -\left(\frac{k_1}{p_1} + \frac{k_2}{p_2} + \cdots + \frac{k_q}{p_q}\right)$$

$$m_1 = -\left(\frac{k_1}{p_1^2} + \frac{k_2}{p_2^2} + \cdots + \frac{k_q}{p_q^2}\right)$$

$$m_{2q-1} = -\left(\frac{k_1}{p_1^{2q}} + \frac{k_2}{p_2^{2q}} + \cdots + \frac{k_q}{p_q^{2q}}\right)$$

which can be solved using $V\Lambda k = -m$ where

$$V=\begin{bmatrix} 1 & 1 & \cdots & 1 \\ \frac{1}{p_1} & \frac{1}{p_2} & \cdots & \frac{1}{p_q} \\ \frac{1}{p_1^2} & \frac{1}{p_2^2} & .. & \frac{1}{p_q^2} \\ . & . & . & . \\ \frac{1}{p_1^{q-1}} & \frac{1}{p_2^{q-1}} & . & \frac{1}{p_q^{q-1}} \end{bmatrix}, \Lambda=\begin{bmatrix} \frac{1}{p_1} & 0 & .. & .. & 0 \\ 0 & \frac{1}{p_2} & 0 & .. & 0 \\ 0 & 0 & . & . & 0 \\ 0 & 0 & .. & \frac{1}{p_{q-1}} & 0 \\ 0 & 0 & 0 & .. & \frac{1}{p_q} \end{bmatrix}, k=\begin{bmatrix} k_1 \\ k_2 \\ . \\ . \\ k_q \end{bmatrix}, m=\begin{bmatrix} m_0 \\ m_1 \\ . \\ . \\ m_{q-1} \end{bmatrix} \tag{59}$$

Thus $k = -\Lambda^{-1}V^{-1}m$ which are the residues of the system. Finaly, the poles obtained in (55) are combined with the residues in (48) to obtain the time domain impulse response in equation (29).

3.3 Adapting AWE to Obtain a Response to a Unit Step Input (integration method):

To avoid computationally expensive explicit convolution, recursive convolution is applied based on the pole-residue representation of the transfer function [12]. For a system described in the Laplace domain as:

$$Y(s) = \frac{k_i}{s+p_i}X(s) \ldots \ldots . \frac{d}{dt}y(t) + p_i y(t) = k_i x(t) \tag{60}$$

Multiply both side by $e^{p_i t}$,

$$\frac{e^{p_i t}dy(t)}{dt} + \ e^{p_i t}p_i y(t) = k_i e^{p_i t}x(t)$$

$$\frac{d}{dt}\left(e^{p_i t}y(t)\right) = k_i e^{p_i t}x(t)$$

$$e^{p_i t_n}y(t_n) - e^{p_i t_{n-1}}t(t_{n-1}) = \int_{t_{n-1}}^{t_n} k_i e^{p\tau}x(\tau)d\tau$$

Assume $x(\tau)$ is piecewise constant x_n over each time interval $[t_n - t_{n-1}]$. Solving equation (49) over a time interval using the recursive solution is:

$$y(t_n) = k_\infty x(t_n) + \sum_{i=1}^{q} y_i'(t_n) \tag{61}$$

where

$$y_i'(t_n) = \int_{t_{n-1}}^{t_n} k_i e^{p\tau}x(\tau)d\tau + e^{-p_i(t_n - t_{n-1})}y_i'(t_{n-1}) \tag{62}$$

The equation in (62) updates the output at t_n using only the previous state $y_i'(t_{n-1})$ and the input $x(t_{n-1})$ eliminating the need to store the entire history of $x(t)$ [10]. Thus, for a unit step response (62) is equal to:

$$y_i'(t_n) = \frac{k_i\left(1 - e^{p_i(t_n - t_{n-1})}\right)}{p_i(t_n - t_{n-1})} + e^{-p_i(t_n - t_{n-1})} y_i'(t_{n-1}) \qquad (63)$$

3.4 Implementation of Y parameters:

Considering the general form derived in equation (17) with $n = 2$. One can generate rational expression from a given Y values of a transmission line as follows:

$$Y_R + jY_i = \frac{a_1 s + a_0}{s^2 + b_1 s + b_0} \qquad (64)$$

At $s = jw$

$$(Y_R + jY_i)(-w^2 + b_1 jw + b_0) = a_1 jw + a_0 \qquad (65)$$
$$(-w^2 Y_R + b_1 jwY_R + b_0 Y_R - w^2 jY_i - b_1 wY_i + jb_0 Y_i) = a_1 jw + a_0$$

Re-write (65) as:

$$(b_1 jwY_R + b_0 Y_R - b_1 wY_i + jb_0 Y_i) - a_1 jw - a_0 = w^2 Y_R + jw^2 Y_i \qquad (66)$$

To find the coefficients the following is applied:

$$A = \begin{bmatrix} -1 & Y_R^1 & 0 & -Y_i^1 w \\ 0 & Y_i^1 & -jw^1 & jwY_R^1 \\ \ldots & .. & .. & .. \\ -1 & Y_R^N & 0 & -Y_i^N w \\ 0 & Y_i^N & -jw^N & -w^2 Y_i^N \end{bmatrix}, B = \begin{bmatrix} a_0 \\ b_0 \\ a_1 \\ b_1 \end{bmatrix} \; and \; C = \begin{bmatrix} Y_R^1 w^2 \\ jY_i^1 w^2 \\ \ldots \\ Y_R^N w^2 \\ jY_i^N w^2 \end{bmatrix} \qquad (67)$$

$where \; A\,B = C \; and \; B = A^{-1}B.$

Once the rational fraction is derived, AWE is used to obtain the response of the transmission line and compare it to the exact results. Moreover, the approach to obtain an efficient model using AWE and Y measurements is as outlined as follows:

3.4.1 Methodology for Rational Approximation Model Construction of TL:

The proposed methodology involves an iterative algorithm to construct a rational approximation model using frequency-domain measurements (Y measurements). The process is outlined as follows:

1. Initial Model Generation: A rational approximation model is generated using the first frequency points at which the frequency is small, and the oscillation is small (e.g., indices 1–5) via the system

identification method described by Equations (42) and (66). This initial model captures the low-frequency behaviour of the system.

2. Residual Calculation: The initial model is evaluated at the subsequent five frequency points (indices 6–10). The difference (residual) between the measured data and the model's prediction at these points is computed to quantify the approximation error.

3. Iterative Model Refinement: A secondary rational approximation is generated from the residual error. This correction term is combined with the initial model to enhance accuracy. The process repeats iteratively: for each subsequent block of five frequency points (e.g., 11–15, 16–20, etc.), the current composite model is evaluated, the residual is calculated, and a new correction model is generated and superimposed. This step continues for until all desired frequency points are covered.

4. Validation Against Exact Solution: After iterating through all designated frequency blocks, the final composite model's frequency response is compared to the exact analytical solution (precomputed at 100 frequency points) to validate accuracy.

Finally, the final model is pruned by applying post-processing techniques to eliminate redundant and unstable poles and residues, thereby improving numerical stability and computational efficiency. These methods are detailed in subsequent sections.

3.5 Complex frequency hopping or Novel feature:

Complex Frequency Hopping (CFH) is an advanced iterative technique for modelling interconnect networks by combining multi-point moment-matching and pole-residue extraction across the complex frequency plane [13]. CFH enhances accuracy over single-point Pade approximations by strategically "hopping" to expansion points near dominant poles, generating localized Taylor series moments, and synthesizing a unified transfer function. This method efficiently captures high-frequency effects in distributed systems (e.g., transmission lines) while avoiding numerical instability and truncation errors inherent in traditional eigenmode-based moment generation [13]. However, experimental implementation and testing revealed limitations in extending CFH to terahertz (THz) models, requiring further investigation. The rapid signal transitions, sensitivity to parasitic effects, and increased computational demands lead to increased errors and numerical rounding issues, especially at high frequencies. These challenges highlight the need for further research into adaptive moment-generation algorithms, enhanced pole-selection criteria, and numerical stability optimizations to tailor CFH for next-generation THz interconnect analysis.

3.6 FRACTIONAL-ORDER TRANSMISSION LINE MODEL:

(next few days) this will depend on what's achieved (improvements and considerations + novel feature)

At THz frequency the following is true:

$$R = R_o + R_s(1 + j)\sqrt{w}$$

The below Figure shows the frequency response with R as a constant and with R as a variable depending on w.

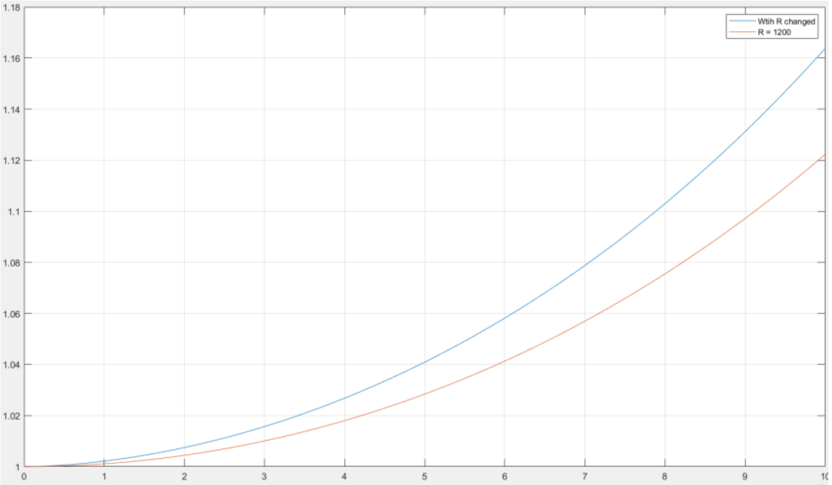

Chapter 4 – Testing, Results and Discussion

This chapter evaluates the accuracy and efficiency of FDTD, RLC ladder networks and AWE with rational expression models in transmission line analysis, comparing them to exact solutions. Using root mean squared error (RMSE) and computational CPU speed as metrics (tic toc on MATLAB), the chapter highlights trade-offs between precision and resource demands. Challenges in transient response, AWE's unit step performance, and enhancements via fractional-order model are explored. The chapter concludes with a comparison and guiding method selection for high-speed circuit design based on accuracy and computational cost.

4.1 FDTD

Code 1 from the appendix is used with the same parameters for all methods and a load of 100 ohms. The following table and figure highlight the main results.

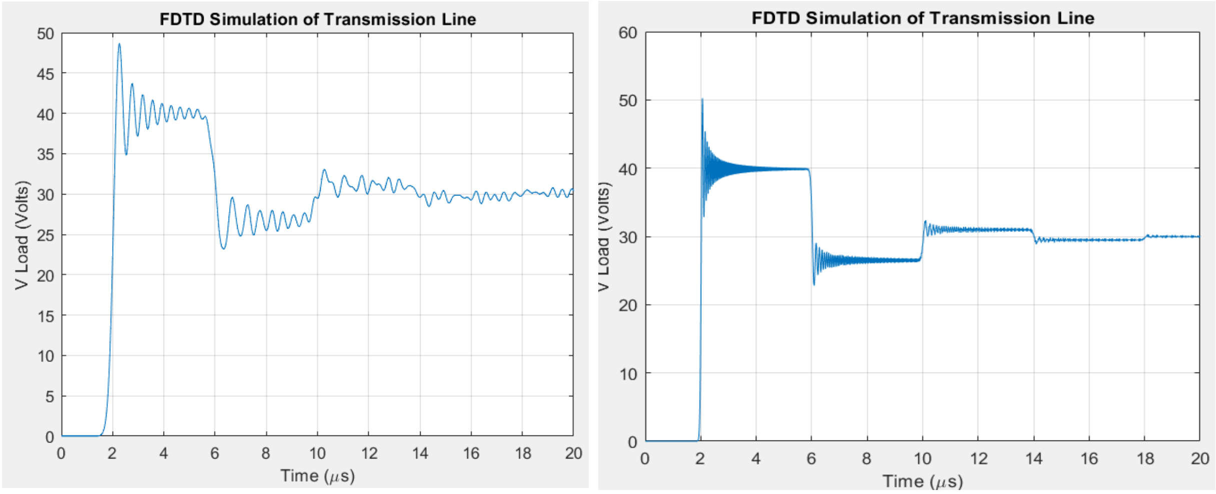

Figure 4.1: FDTD simulation of a transmission line with a 100 Ω load. The left plot corresponds to a discretization of 20 sections, while the right plot uses 200 sections.

Table 1: Comparison of the FDTD method and time taken across different numbers of sections.

Number of sections	Time taken
20	0.0851
100	0.1220
200	0.3180

The Finite-Difference Time-Domain (FDTD) method demonstrates a clear trade-off between accuracy and computational efficiency. As the number of sections increases, the time required for computation grows significantly. For instance, at 200 sections, the time taken is approximately 2.86 seconds, which is much higher compared to the RLC ladder network. The requirement of a very small-time step to maintain accuracy further adds to its computational burden, making it less efficient for large-scale simulations.

4.2 RLC ladder

Code 2 from the appendix is used with the same parameters as in FDTD. The following table and figure show the key results.

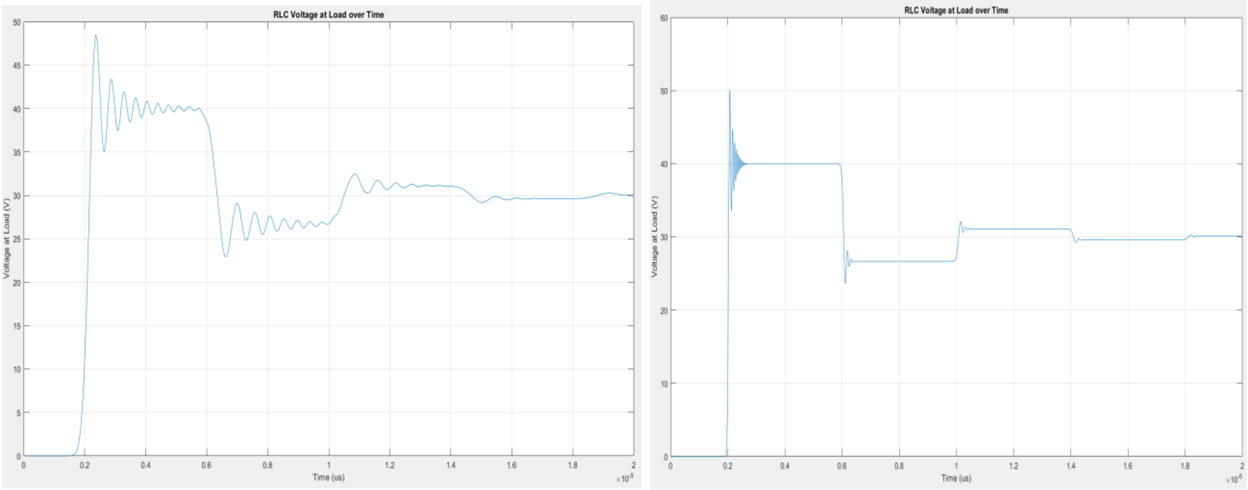

Figure 4.2: Voltage response of an RLC circuit over time using different discretization levels. The left plot corresponds to 20 sections, while the right plot uses 200 sections.

Table 2: Comparison of the RLC method and time taken across different numbers of sections.

Number of sections	Time taken
20	0.0224
100	0.0325
200	0.0515

It was observed that the RLC ladder network, particularly when solved using ode23, was characterized by significantly better computational efficiency compared to FDTD. It was found that even as the number of sections increased, the time required remained relatively low, with 0.0224 seconds recorded for 20 sections, 0.0325 seconds for 100 sections, and 0.0515 seconds for 200 sections. This efficiency was attributed to the variable time-step approach of ode23, which was observed to adapt dynamically to the system's behaviour and reduce unnecessary computations. Furthermore, it was demonstrated that the use of ode23 for transmission line analysis yielded results that were both more accurate and faster compared to those obtained with ode45. It was also shown through fixed time-step analysis that the RLC method performed better in terms of both accuracy and speed when compared to FDTD.

4.3 Exact solution compared with FDTD, RLC and challenges.

4.3.1 Exact solution:

The exact transmission line model for an open-circuit design is derived using equation (26) or (28). By assuming a lossless line and applying the same parameters as those used in the RLC and FDTD methods, the following results are obtained using code 6 in the appendix. These results are then compared against other models to evaluate their accuracy and computational performance.

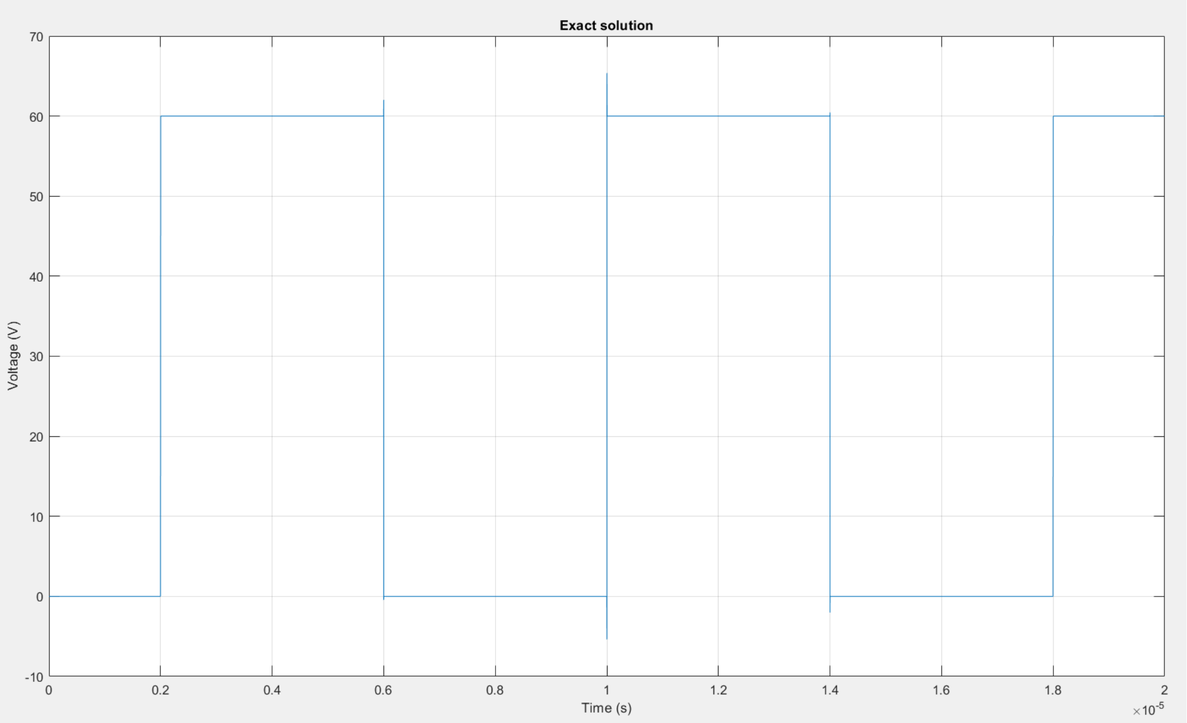

Figure 4.3: Simulation of the exact solution of a lossless transmission line with an open-circuit termination and a 30V input.

The result in Figure 4.3.1 is expected since the input voltage is 30V, and the transmission line is open-circuited, meaning there is no load. As a result, the wave propagates forward and then reflects backward, leading to a superposition of the incident and reflected waves. This interaction creates a square-like waveform with a peak voltage of 60V, given by $V = V^{+} + V^{-}$.

4.3.2 RLC and FDTD

A fixed time step of $1x10^{-8}$ and $1x10^{-10}$ seconds is used for the RLC and FDTD methods respectively. The table below compares the efficiency of the Finite-Difference Time-Domain (FDTD) method and the RLC ladder network in terms of Root Mean Square Error (RMSE) and computation time.

Table 3: Comparison of the RLC ladder network and FDTD method across different numbers of sections.

Number of sections	RLC ladder		FDTD	
	Error (RMSE)	time	Error (RMSE)	time
50	9.5367	0.0195	7.2430	0.1142
100	6.9623	0.0395	5.3862	0.1819
200	5.0097	0.0961	5.0746	0.3025
400	3.5005	0.2088	3.2992	0.5047
600	2.8838	0.3722	2.8989	0.8201

It was observed that when a fixed time step was used for the RLC method, it consistently outperformed FDTD in terms of computational speed while maintaining comparable accuracy. For example, at 400 sections, the RLC method required 0.2088 seconds, compared to 0.5047 seconds for FDTD. The RMSE values indicated that FDTD achieved slightly better accuracy in certain cases (e.g., 5.0746 for 200 sections versus 5.0097 for RLC), but the considerable difference in computation time rendered the RLC method the more practical choice. In addition, it was demonstrated that the RLC method, which does not rely on a small-time step, can be scaled efficiently for higher accuracy.

4.3.3 Visual inspections of all solutions (methods)

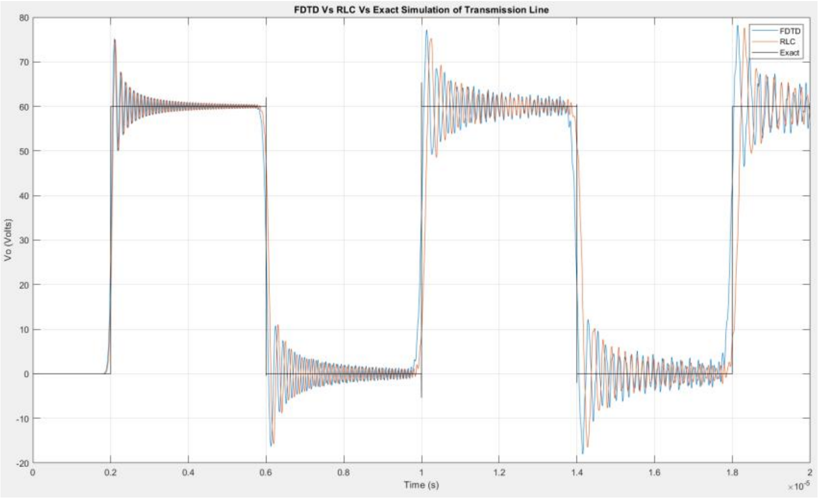

Figure 4.4: Comparison of FDTD, RLC ladder, and exact simulation of a transmission line, showing output voltage Vo over time with numerical oscillations.

4.3.4 FDTD and magic time step:

4.4 THz Results:

This test evaluates the model's response to three distinct input types: a unit step input, a sine wave with a THz frequency, and a trapezoidal pulse input. The trapezoidal pulse has a rise time of 1 ps from 0 to 1 V, a fall time of 1 ps, and remains at 1 V for 5 ps. The results are based on the following lumped transmission line (TL) parameters.

$C = 1x10^{-10}F, \qquad L = 250x10^{-9}H, \qquad R = 1200Ohms, \qquad l = 150x10^{-6}m, \qquad R_s = 10$

4.4.1 FDTD modification:

In the FDTD method, the equations derived in (2a) and (2b) correspond to the lossless case. To account for a lossy transmission line with per-unit-length parameters and the source resistance R_s , the following modified equations are derived and applied based on [4].

Voltage for k = 1 (at the source) is:

$$V_1^{n+1} = \frac{(R_s \frac{C}{2}\frac{\Delta z}{\Delta t} - \frac{1}{2})V_1^n - \ R_s\left(I_1^{n+\frac{1}{2}}\right) + \frac{(V_s^{n+1} + V_s^n)}{2}}{R_s \frac{C}{2}\ \frac{\Delta z}{\Delta t} + \frac{1}{2}} \qquad (68a)$$

For k = 2, ..,NDZ.

$$V_k^{n+1} = V_k^n - \frac{\Delta t}{\Delta z C}\left(I_k^{n+\frac{1}{2}} - I_{k-1}^{n+\frac{1}{2}}\right) - \frac{G\Delta t}{C}V_k^n. \tag{68b}$$

if $G\ = 0$, then equation (68b) is identical to the equation for the lossless case, as given in equation (2a).

At K = NDZ+1 the voltage depends on R_L, and should therefore be the same as in the lossless case:

$$V_{NDZ+1}^{n+1} = \frac{(R_L \frac{C}{2}\frac{\Delta z}{\Delta t} - \frac{1}{2})V_{NDZ+1}^n -\ R_L\left(I_{NDZ}^{n+\frac{1}{2}}\right) + \frac{(V_L^{n+1} + V_L^n)}{2}}{R_L \frac{C}{2}\frac{\Delta z}{\Delta t} + \frac{1}{2}} \tag{68c}$$

Finaly, the current update for all nodes (K=1,…,NDZ):

$$I_k^{n+\frac{3}{2}} = I_k^{n+\frac{1}{2}} - \frac{\Delta t}{\Delta z l}(V_{k+1}^{n+1} - V_k^{n+1}) - \frac{R\Delta t}{l}I_k^{n+\frac{1}{2}} \tag{68d}$$

These modifications to accommodate the lossy case are implemented in Code 7 in the appendix and are consequently applied in generating the following results.

4.4.2- The unit step response:

In this section, the impact of incorporating a source resistance R_s is investigated, highlighting its influence on both computational efficiency and signal accuracy. The inclusion of R_s introduces additional damping into the system, thereby altering the energy dissipation and the effective impedance, which in turn affects the overall performance and error metrics.

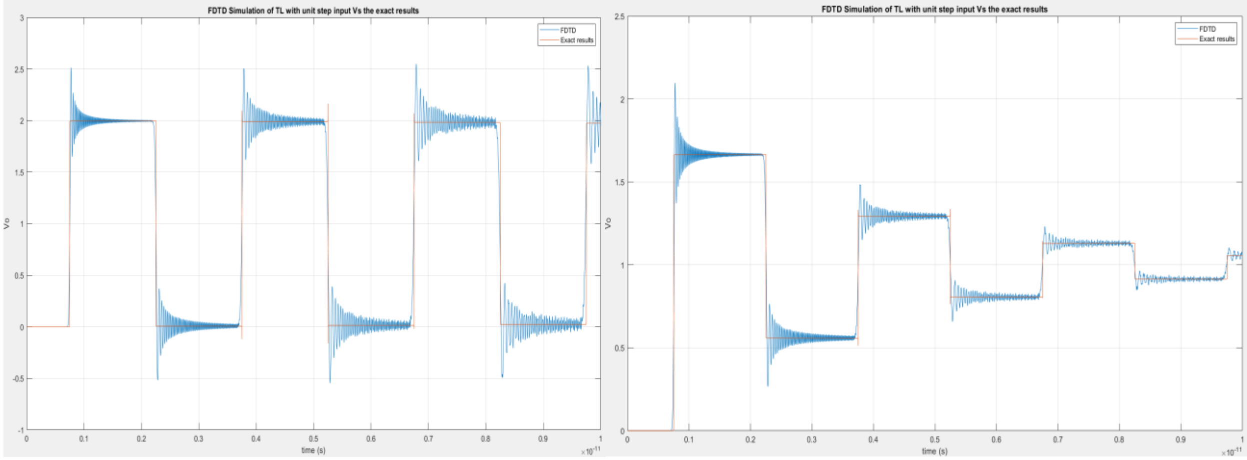

Figure 4.5: Comparison of FDTD simulation results with exact solutions for a transmission line with unit step input. The left plot represents the case without source resistance Rs, while the right plot includes Rs.

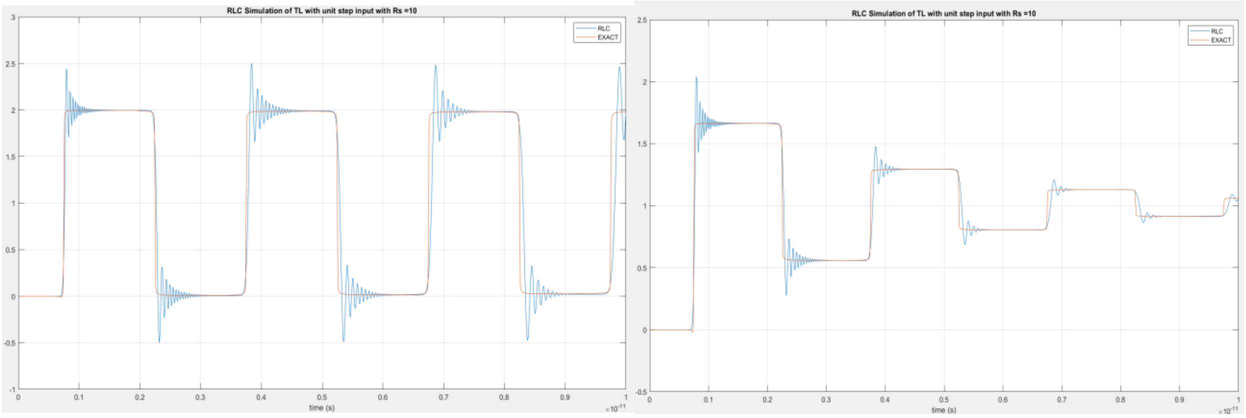

Figure 4.6: Comparison of RLC simulation results with exact solutions for a transmission line with a unit step input. The left plot represents the case without source resistance Rs, while the right plot includes Rs.

Table 4: Comparison of the RLC ladder network and FDTD method across different numbers of sections.

Number of sections	RLC			FDTD		
	Error	Error (Rs)	CPU time	Error	Error (Rs)	CPU time
50	0.3609	0.0998	0.01472	0.2905	0.0836	0.02410
100	0.2516	0.0701	0.02402	0.2060	0.0658	0.04670
200	0.1718	0.0481	0.04665	0.1535	0.0524	0.09126
400	0.1180	0.0333	0.12205	0.1188	0.0421	0.19728

The changes observed when Rs is added are attributed to the additional damping effect it introduces. This damping modifies the transmission line's characteristic impedance and reduces the amplitude of transient oscillations. Consequently, the unit step response is altered, leading to variations in the RMSE errors, as the system dynamics adjust to the resistive influence.

4.4.3- Response to a sine wave input at THz frequency:

This section presents the results of using different model if the input is a sine wave at 100 GHz frequency.

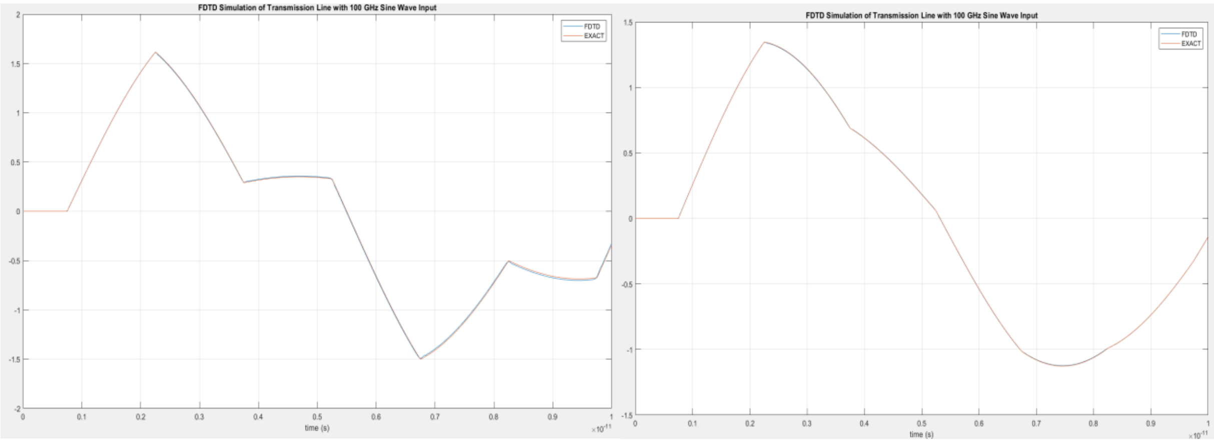

Figure 4.7: Comparison of FDTD simulation results with exact solutions for a transmission line with a sine wave at THz input. The left plot represents the case without source resistance Rs, while the right plot includes Rs.

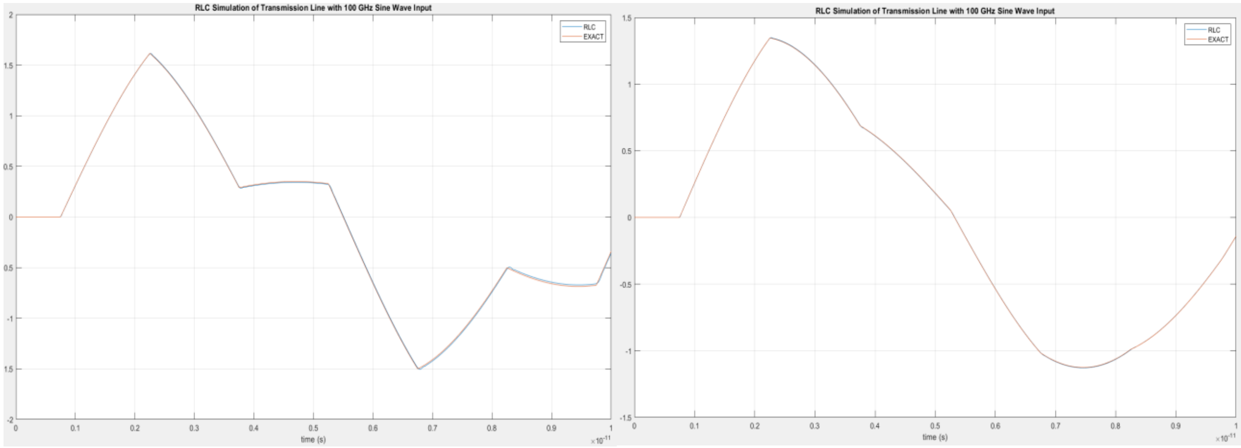

Figure 4.8: Comparison of RLC simulation results with exact solutions for a transmission line with a sine wave at THz input. The left plot shows the case without source resistance Rs, while the right plot includes Rs.

Table 5: Comparison of the RLC ladder network and FDTD method across different numbers of sections with sine wave at THz frequency input.

Number of sections	RLC			FDTD		
	Error	Error (Rs)	CPU time	Error	Error (Rs)	CPU time
50	0.0383	0.0079	0.00716	0.0372	0.0076	0.02410
100	0.0193	0.0039	0.01243	0.0188	0.0038	0.04670
200	0.0097	0.0020	0.02890	0.0095	0.0019	0.09126
400	0.0049	9.8518e-04	0.07670	0.0047	9.6461e-04	0.19728

The inclusion of R_s introduces damping effects, altering the system's transient behaviour and error metrics, as reflected in Table 5. This table demonstrates that both RLC ladder networks and FDTD methods achieve lower errors (e.g., 0.0047 for FDTD at 400 sections) as the number of sections increases, though FDTD requires more CPU time. The analysis underscores the trade-offs between accuracy and computational efficiency when modelling high-frequency signals under resistive influences.

4.4.4- Response due to Trapezoidal pulse:

A trapezoidal pulse that:

- Rises linearly from 0 V to 1 V over 1 ps,
- Stays at 1 V for 5 ps,
- Falls back to 0 V over 1 ps,
  can be built from ramps and exponentials in the Laplace domain.

Time-Domain Definition

$$v_{pulse}(t) = \left\{\begin{matrix} 0, & t < 0 \\ linear\ rise, & 0 \le t < 1ps \\ 1, & 1ps \le t < 6ps \\ linear\ fall, & 6ps \le t < 7ps \\ 0, & t \ge 7ps. \end{matrix}\right\} \quad (69)$$

Total duration: 7 ps = 1 ps (rise) + 5 ps (high) + 1 ps (fall).

constructing equation (69) via Ramp Functions as follows:

$$ramp(t) = t\,u(t)\,, in\ laplace\ domin\,\frac{1}{s^2}. \quad (70)$$

A linear rise and fall from 0 to 1 over $[0, T_r]$ can be written as

$$\frac{1}{T_r}\,[ramp(t) - ramp(t - T_r)] \quad (71)$$

Hence, for rise time T_r and peak duration T_P

$$v_{pulse}(t) =$$

$$\frac{1}{T_r}[ramp(t) - ramp(t - T_r)] - \frac{1}{T_r}\left[ramp\left(t - \left(T_r + T_p\right)\right) - ramp\left(t - \left(2T_r + T_p\right)\right)\right] \quad (72)$$

using $\mathcal{L}\{ramp(t - a)\} = \frac{e^{-as}}{s^2}$, we get:

$$V_{pulse}(s) = \frac{1}{T_r s^2}[1 - e^{-T_r s}] - \frac{1}{T_r s^2}\left[e^{(-T_r+T_p)s} - e^{(-2T_r+T_p)s}\right]. \quad (73)$$

Then $V_{pulse}(s)$ is used for obtaining the exact solution using NILT while $v_{pulse}(t)$ (code 8 in the appendix) is used for RLC and FDTD methods to obtain the following results.

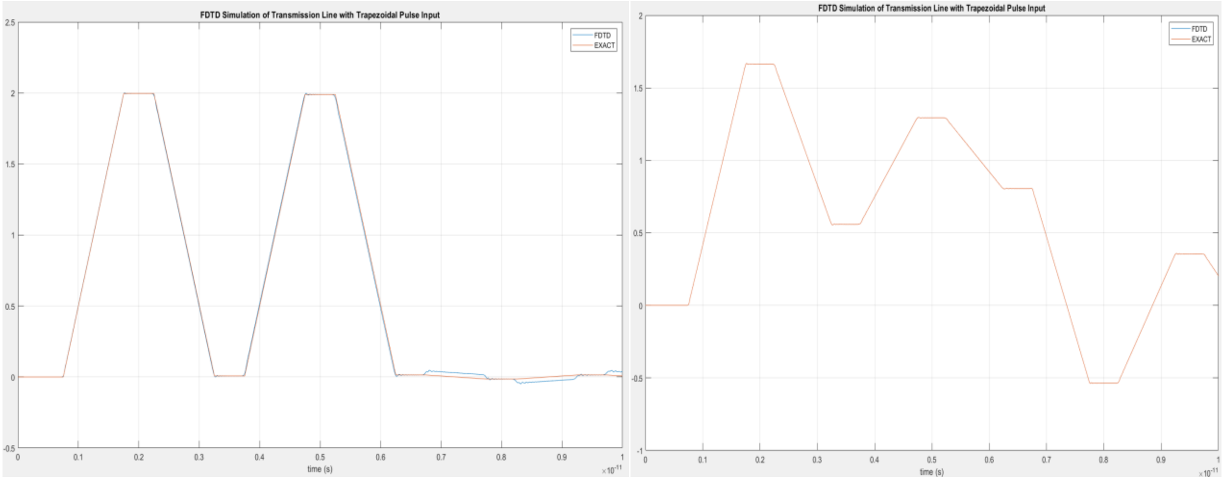

Figure 4.9: Comparison of FDTD simulation results with exact solutions for a transmission line with a pulse input. The left plot represents the case without source resistance Rs, while the right plot includes Rs.

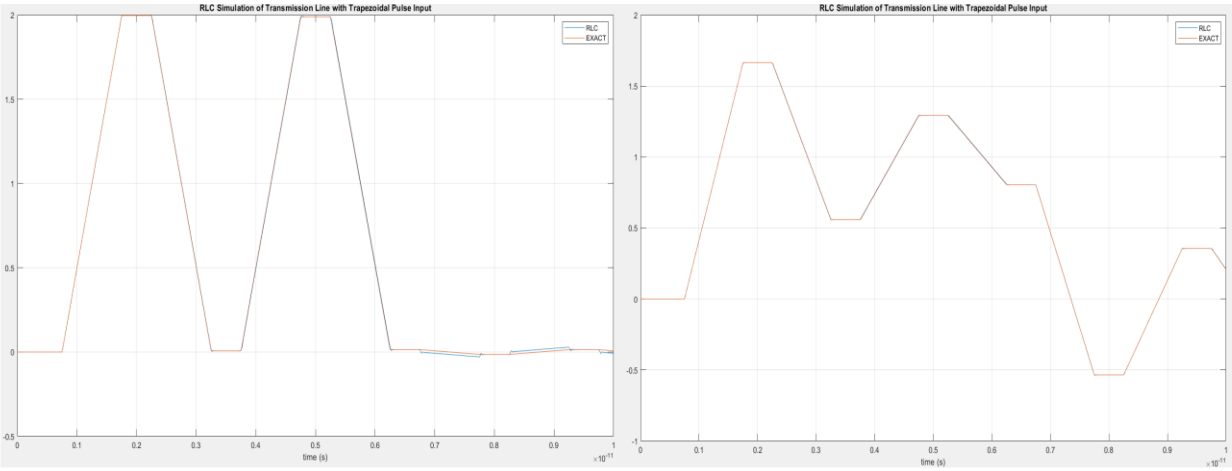

Figure 4.10: Comparison of RLC simulation results with exact solutions for a transmission line with a pulse input. The left plot represents the case without source resistance Rs, while the right plot includes Rs.

Table 6: Comparison of the RLC ladder network and FDTD method across different numbers of sections with trapezoidal pulse input.

Number of sections	RLC			FDTD		
	Error	Error (Rs)	CPU time	Error	Error (Rs)	CPU time
50	0.0700	0.0157	0.00716	0.0690	0.0151	0.14985
100	0.0353	0.0078	0.01243	0.0347	0.0076	0.14901

200	0.0177	0.0039	0.02890	0.0174	0.0038	0.22378
400	0.0089	0.0020	0.07670	0.0087	0.0019	0.32909

This section analyses the response of transmission line models to a trapezoidal pulse input, defined with a 1 ps linear rise to 1 V, a 5 ps plateau, and a 1 ps linear fall. The pulse is mathematically constructed in the Laplace domain using ramp functions (Equations 70–73), combining exponential terms to represent its linear transitions. Simulations using RLC ladder networks and FDTD methods are compared in Table 6, which shows decreasing errors (e.g., RLC error drops from 0.0700 to 0.0089 as sections increase from 50 to 400) but rising computational costs, particularly for FDTD (CPU time increases from 0.14985 to 0.32909). Figures 4.9 and 4.10 illustrate the impact of source resistance R_s, where its inclusion introduces damping effects, aligning simulations closer to exact solutions. The analysis highlights the trade-off between model accuracy and computational efficiency, emphasizing how resistive components refine transient behavior in high-speed pulse applications.

4.5 AWE testing

4.5.1 Impulse response:

Consider the following example:

$$A = \begin{bmatrix} -2 & 1 & 0 & 0 \\ 1 & -2 & 1 & 0 \\ 0 & 1 & -2 & 1 \\ 0 & 0 & 1 & -1 \end{bmatrix}, B = \begin{bmatrix} 1 \\ 0 \\ 0 \\ 0 \end{bmatrix} \, and \; C = \begin{bmatrix} 1 \\ 0 \\ 0 \\ 0 \end{bmatrix} \qquad (74)$$

One can find the impulse response by calculation moments, poles and residues using equations (51), (55) and (58) respectively,

$$m_0 = 1 \, , m_1 = -4, m_2 = 30, m_3 = \, -246, m_4 = 2037, m_5 = -16886, m_6 = 140000$$

$$p_1 = -3.53, p_2 = -2.35, p_3 = -1, p_4 = -0.12$$

$$k_1 = 0.18, k_2 = 0.43, k_3 = 0.33, k_4 = 0.05$$

Then the impulse response is:

$$H(t) = \; 0.18e^{-3.53t} \, + \, 0.43e^{-2.35t} + 0.33e^{-t} + \, 0.05e^{-0.12t} \qquad (75)$$

4.5.2 A theoretical method for validating AWE [11].

The impulse response of a state space model is given by:

$$y(t) = Ce^{at}B \tag{76}$$

$$where, \quad e^{at} = Me^{\Omega t}M^{-1}$$

$$and\ \Omega = M^{-1}AM = \begin{bmatrix} \lambda_1 & 0 & 0 \\ \dots & \lambda_2 & 0 \\ 0 & \dots. & \lambda_n \end{bmatrix}$$

Considering the same example with $t = 0{:}\,2$ with time step of 0.001 the following is obtained:

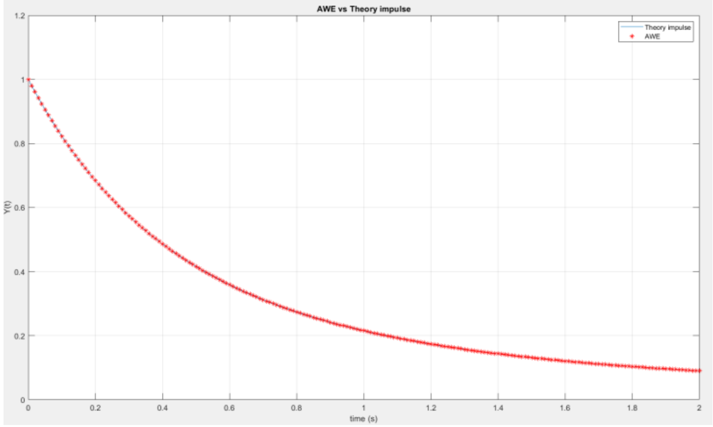

Figure 1.11: Comparison of AWE approximation and theoretical impulse response,

The Asymptotic Waveform Evaluation (AWE) method is tested using a system matrix approach, generating moments, poles, and residues to derive the impulse response function. The obtained RMSE value of $5.6523x10^{-8}$ indicates high accuracy, suggesting that AWE is a highly reliable method for transmission line analysis.

4.5.3-Unit step response.

Using the same example in (74),

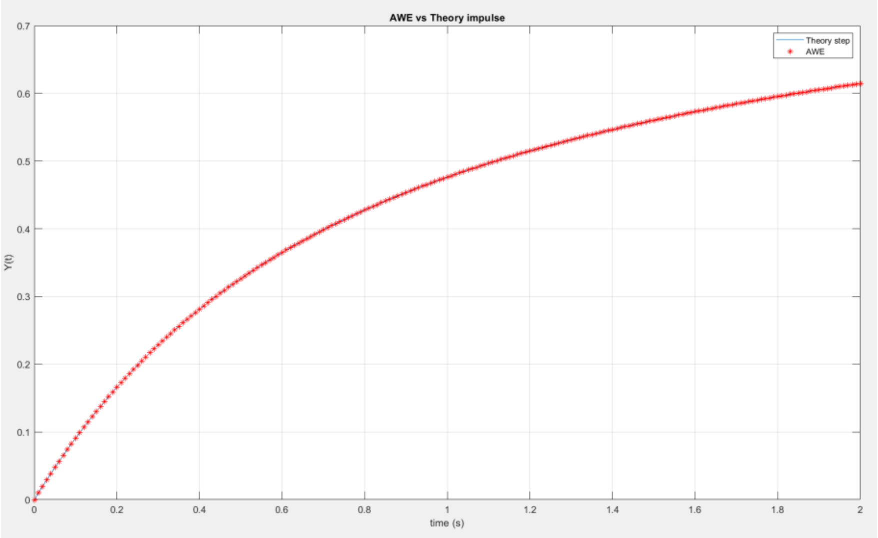

Figure 4.12: Comparison of AWE and the theoretical step response over time shows that AWE closely aligns with the theoretical model, highlighting its accuracy.

Similar to its impulse response, the unit step response of AWE also demonstrates exceptional accuracy, with an RMSE of $1.2973x10^{-8}$. The results highlight that reducing the time step further enhances AWE's accuracy, though at the cost of increased computational time.

4.6 Transmission Line Testing Using Asymptotic Waveform Evaluation.

This section implements the methodology described in Section 3.4 to construct an AWE model for transmission line analysis, utilizing Y-parameter measurements and step response for validation. The model is simulated using code 12 in the Appendix, configured with the following transmission line parameters:

$$C = 1x10^{-10}F, \qquad L = 250x10^{-9}H, \qquad R = 0.1\ Ohms, \qquad l = 400m,$$

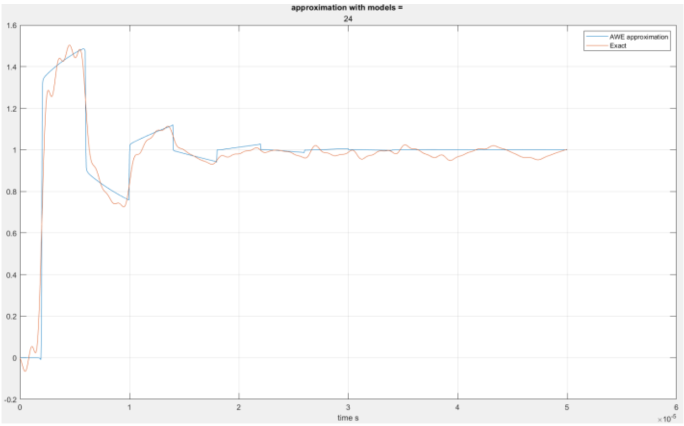

Figure 4.13: shows the step response of the generated AWE model compared to the exact results.

Figure 4.13 illustrates the step response of the AWE model against exact solutions, demonstrating strong agreement with (RMSE) of 0.0869 (unit step) and 0.4269 (impulse response). However, during experimental validation, computational challenges arise when computing moments at terahertz (THz) frequencies due to numerical instability. To address this, the rank of the system matrix **A** is analysed. If the matrix rank is found to be lower than its dimension, adopting a first-order rational approximation—instead of the conventional second-order approach—effectively alleviates rounding errors and improves numerical accuracy. This adjustment ensures higher accuracy in modelling high-frequency behaviour at THz ranges, while maintaining computational reliability.

(next few days) this will depend on what's achieved.

- **Comparing all methods in terms of accuracy and cpu speed.**
- **Applying fractional-order model.**

Chapter 6 – Ethics

Engineering ethics play a crucial role in the responsible development and implementation of technology. This project, which focuses on the simulation and exploration of terahertz (THz) transmission lines, adheres the ethical principles outlined in the IEEE Code of Ethics, the Engineers Ireland (IEI) Code of Ethics, and best practices in software usage, ensuring fairness, integrity, and professionalism throughout the research process.

6.1 IEEE Code of Ethics

The IEEE Code of Ethics [15] highlights the importance of integrity, safety, fairness, and professional responsibility in engineering practices. In alignment with these principles, the following ethical considerations were observed throughout this project:

- **Public Safety and Welfare:** The research was conducted with a focus on minimizing risks to public welfare, ensuring transparency in reporting findings, and considering the broader impact of THz technology.
- **Honest Representation of Results:** All data, simulations, and conclusions have been presented accurately, avoiding any misleading claims or misinterpretations.
- **Proper Credit and Acknowledgment:** Previous research, methodologies, and contributions from other professionals have been properly cited to maintain intellectual integrity.
- **Avoiding Conflicts of Interest:** The work was conducted objectively, with no external influence affecting the outcomes.

6.2 Engineers Ireland (IEI) Code of Ethics

As a professional engineering project, this work also follows the Engineers Ireland (IEI) Code of Ethics [16], which mandates professional responsibility and adherence to high ethical standards. The key IEI ethical principles applied in this project include:

- **Commitment to Public Safety and Environmental Protection:** The research was conducted responsibly, ensuring that findings contribute positively to engineering knowledge without causing harm.
- **Professional Competence and Integrity:** The project was executed within the researcher’s field of expertise, with clear communication of results and limitations.

- **Fairness, Courtesy, and Good Faith:** All collaborations and academic discussions were conducted respectfully and professionally, upholding ethical engineering standards.

6.3 Use of Licensed MATLAB and Software for Implementation and Testing.

In compliance with ethical engineering practices and software licensing agreements, this project exclusively used licensed versions of MATLAB and other required software for simulation, testing, and implementation [17]. This aligns with professional engineering standards, ensuring:

- **Legal and Ethical Software Usage:** Unauthorized or pirated software was strictly avoided, maintaining compliance with intellectual property laws.
- **Reliability and Accuracy of Results:** Using licensed software ensured that the simulations and calculations were performed using verified, up-to-date tools, minimizing errors and inaccuracies.
- **Multiple Testing for Accuracy:** The achieved results were tested multiple times using different parameter variations to ensure accuracy and reliability
- **Adherence to Industry Standards:** The project follows the best practices in software implementation to ensure high-quality, reproducible research outcomes.

By adhering to these ethical principles, this project upholds professional engineering standards, ensuring responsible and ethical research in THz transmission line modeling.

Chapter 7 - Conclusions and Further Research

This project evaluated the effectiveness of numerical methods for modelling terahertz (THz) transmission lines, focusing on balancing computational efficiency and accuracy. The Finite-Difference Time-Domain (FDTD) method provided foundational insights into transient and steady-state behaviours but proved computationally intensive, with simulation times escalating to 16.83 seconds for 400 sections. In contrast, the RLC ladder network, solved using MATLAB's adaptive ode45 solver, demonstrated superior efficiency, completing 200-section simulations in 0.127 seconds while maintaining competitive accuracy (RMSE: 5.5411 vs. FDTD's 5.0746 at 200 sections). The Numerical Inverse Laplace Transform (NILT) exact solution validated both methods, confirming their alignment with theoretical expectations for lossless lines. Asymptotic Waveform Evaluation (AWE) emerged as a highly accurate technique for transient analysis, achieving RMSE values as low as 1.2973×10^{-8} for step responses, though its computational cost increased with finer time steps.

This work contributes to the advancement of THz communication systems by demonstrating that RLC ladder approximations and AWE offer practical, scalable solutions for high-frequency applications. For large-scale simulations requiring rapid results, the RLC method is optimal, while AWE excels in scenarios demanding precise transient analysis. The integration of Y-parameters and pole-residue models further enhances the reliability of these tools for designing next-generation technologies such as 6G networks and biomedical imaging systems.

This will depend on what's achieved.

References

1. T. Kürner, "Turning THz Communications into Reality: Status on Technology, Standardization and Regulation," *IRMMW-THz 2018 - 43rd International Conference on Infrared, Millimeter, and Terahertz Waves*, Nagoya, Japan, 2018, pp. 1-2, doi: 10.1109/IRMMW-THz.2018.8510317.
2. X. Mou, Y. Chen, C. Ma, Y. Che, and J. He, "A numerical method to simulate THz-wave generation and detection of field-effect transistors," in *Proc. IEEE*, 2008, p. 1, doi: 10.1109/IRMMW-THz.2008.2186.
3. D. M. Pozar, *Microwave Engineering*, 4th ed. Hoboken, NJ, USA: Wiley, 2012, pp. 48–50.
4. C. R. Paul, "Incorporation of terminal constraints in the FDTD analysis of transmission lines," in *IEEE Transactions on Electromagnetic Compatibility*, vol. 36, no. 2, pp. 85-91, May 1994, doi: 10.1109/15.293284.
5. Y. Shang, H. Yu and W. Fei, "Design and Analysis of CMOS-Based Terahertz Integrated Circuits by Causal Fractional-Order RLGC Transmission Line Model," in *IEEE Journal on Emerging and Selected Topics in Circuits and Systems*, vol. 3, no. 3, p. 355, Sept. 2013, doi: 10.1109/JETCAS.2013.2268948.
6. E. Gad, Y. Tao and M. Nakhla, "Fast and Stable Circuit Simulation via Interpolation-Supported Numerical Inversion of the Laplace Transform," in *IEEE Transactions on Components, Packaging and Manufacturing Technology*, vol. 12, no. 1, pp. 121-130, Jan. 2022, doi: 10.1109/TCPMT.2021.3122840.
7. L. Brancik, "Matlab based time-domain simulation of multiconductor transmission line systems," *The IEEE Region 8 EUROCON 2003. Computer as a Tool.*, Ljubljana, Slovenia, 2003, pp. 464-468 vol.1, doi: 10.1109/EURCON.2003.1248066.
8. L. Brančík, "Numerical Inverse Laplace Transforms for Electrical Engineering Simulation," in MATLAB for Engineers – Applications in Control, Electrical Engineering, IT and Robotics, K. Perutka, Ed. InTech, 2011, pp. 51-56. Available: https://doi.org/10.5772/2468.
9. W. T. Smith and S. K. Das, "Application of asymptotic waveform evaluation for EMC analysis of electrical interconnects," *Proceedings of International Symposium on*

Electromagnetic Compatibility, Atlanta, GA, USA, 1995, pp. 429-434, doi: 10.1109/ISEMC.1995.523595.

10. M. Condon, *Lecturer Notes*, 2025.
11. M. Condon, *System Notes 2023*. Dublin, Ireland: Dublin City University, 2023, pp. 11–14.
12. W. T. Beyene and J. E. Schutt-Ainé, "Efficient transient simulation of high-speed interconnects characterized by sampled data," *IEEE Transactions on Components, Packaging, and Manufacturing Technology—Part B*, vol. 21, no. 1, pp. 105-114, Feb. 1998.
13. E. Chiprout and M. S. Nakhla, "Analysis of interconnect networks using complex frequency hopping (CFH)," *IEEE Transactions on Computer-Aided Design of Integrated Circuits and Systems*, vol. 14, no. 2, pp. 186-200, Feb. 1995.
14. F. Vandrevala, "Transmission Line Model for Material Characterization using Terahertz Time-Domain Spectroscopy," *Ph.D. dissertation*, Univ. of Virginia, July 2019.
15. IEEE, "IEEE Code of Ethics," IEEE, Jun. 2020. Available: https://www.ieee.org/about/corporate/governance/p7-8.html.
16. Engineers Ireland, "Code of Ethics," Engineers Ireland, Feb. 2023. Available: https://www.engineersireland.ie.
17. MathWorks, “Policies and Statements.” Available: https://www.mathworks.com/company/aboutus/policies_statements.html. Accessed: Mar. 10, 2025.

Appendix

Code 1 (FDTD)

```
clear
clc
% a lossless , two-conductor line with Vs(t)=30,
% Rs = 0 R, VL(t) = 0, and RL = 100 R. The line is of
% length L = 400 m and has TJ = 2 x 10' m/s and ZC = 50 R
%%%%%%%%%%%%%%%%%%%%%%%%%%%%%%%%%%%%%%%%%%%%%%%%%%%%%%%%%%%%%%%%
L_total = 400;  % Total length of the line (m)
Zc = 50;  % Characteristic impedance (Ohms)
v = 2e8;  % Speed of propagation (m/s)
Rs = 0;  % Source resistance (Ohms)
RL = 100;  % Load resistance (Ohms)
Vs = 30;%  % Input voltage (V)
% Compute inductance and capacitance
C = 1 / (v * Zc);
L = Zc/v;
NDZ = 20;  % Number of spatial steps
dz = L_total / NDZ;  % Spatial step delta z
dt = 1e-11;  % Time step delta t
t_max = 20e-6;  % Maximum simulation time (20 as in the paper)
t_steps = round(t_max / dt);  % Number of time steps
% allocate voltage and current arrays
V = zeros(NDZ+1, t_steps);
V(1,:)=Vs*ones(1,t_steps);
I = zeros(NDZ, t_steps);
% FDTD Loop for Time Stepping
for n = 1:t_steps-1
    V(1,n+1) = V(1,n);
    for k = 1:NDZ
    if k>1
        V(k,n+1) = V(k,n) + dt/(dz *C)* (I(k-1,n) - I(k,n));  % Update voltage
        I(k-1,n+1) = I(k-1,n)-(dt/(L*dz))*(V(k,n+1)-V(k-1,n+1));% Update current
    end
    end
    V(NDZ,n+1) =V(NDZ,n)+dt*(I(NDZ-1,n)/(C*dz)-V(NDZ,n)/(RL*C*dz));
end

% Plot the results for the voltage at the load
figure(1)
plot((0:t_steps-1)*dt/1e-6, V(NDZ,:));
xlabel('Time (\mus)');
ylabel('V Load (Volts)');
title('FDTD Simulation of Transmission Line');
grid on;
```

Code 2 (RLC)

```
clear
clc
len=400;
N = 20; % Number of sections in the transmission line
dz=len/N;
L = 2.5e-7*dz;   % Inductance
C = 1e-10*dz;    % Capacitance
R = 0;       % Resistance per section
```

```
Rs = 0;       % Source resistance
Rl = 100;     % Load resistance
Vs  = 30;      % Source voltage (could be a function of time)
y0 = zeros(2 * N, 1);
tspan = [0 20e-6];
% Solve using ode23 which shows better result in TL than ode45
[t, y] = ode23(@(t, y) fline(t, y, N, L, C, R, Rs, Rl, Vs), tspan, y0);
% Plot voltage at the end of the transmission line (VN)
figure(1);
plot(t, y(:,N*2));  % Plot voltage at the load (VN)
xlabel('Time (us)');
ylabel('Voltage at Load (V)');
title('RLC Voltage at Load over Time');
grid on
```

Code 3 (fline function)

```
function df = fline(t, y,N,L,C,R,Rs,Rl,Vs)
    % the use of t involves input dependent on time (i.e, sin(t))
    df = zeros(2 * N, 1);
    % Currents and voltages
    In = y(1:2:2*N);  % Currents
    Vn = y(2:2:2*N);  % Voltages
    % Boundary conditions at the source end (n=1)
    df(1) = (-1 / L) * Vn(1) - (Rs + R) / L * In(1) + (1 / L) * Vs;  % dI1/dt
    df(2) = (1 / C) * In(1) - (1 / C) * In(2);  % dV1/dt
    % Interior sections (n=2 to N-1)
    for n = 1:N-1
        df(2*n + 1) = (-1 / L) * Vn(n+1) - R / L * In(n)+(1 / L) * Vn(n);  % dIn/dt
        df(2*n) = (1 / C) * In(n) - (1 / C) * In(n+1);  % dVn/dt
    end
    df(2*N-1) = (-1 / L) * Vn(N) - R / L * In(N) + (1 / L) * Vn(N-1);
    df(2*N) = (1 / C) * In(N) - Vn(N) / (Rl * C);  % dVN/dt (voltage at the load)
end
```

Code 4 (NILTcv)

```
function [ft,t]=niltcv(F,tm,depict);
alfa=0; M=2506; P=3; Er=1e-10; % adjustable
N=2*M; qd=2*P+1; t=linspace(0,tm,M); NT=2*tm*N/(N-2);
omega=2*pi/NT;
c=alfa+log(1+1/Er)/NT; s=c-i*omega*(0:N+qd-1);
Fs(:,:,1)=feval(F,s); Fs(:,:,2)=feval(F,conj(s)); lv=size(Fs,1);
ft(:,:,1)=fft(Fs(:,:,1),N,2); ft(:,:,2)=N*ifft(Fs(:,:,2),N,2);
ft=ft(:,1:M,:);
D=zeros(lv,qd,2); E=D; Q=Fs(:,N+2:N+qd,:)./Fs(:,N+1:N+qd-1,:);
D(:,1,:)=Fs(:,N+1,:); D(:,2,:)=-Q(:,1,:);
for r=2:2:qd-1
 w=qd-r;
 E(:,1:w,:)=Q(:,2:w+1,:)-Q(:,1:w,:)+E(:,2:w+1,:);
 D(:,r+1,:)=-E(:,1,:);
 if r>2
 Q(:,1:w-1,:)=Q(:,2:w,:).*E(:,2:w,:)./E(:,1:w-1,:);
 D(:,r,:)=-Q(:,1,:);
 end
end
A2=zeros(lv,M,2); B2=ones(lv,M,2); A1=repmat(D(:,1,:),[1,M,1]);
B1=B2; z1=repmat(exp(-i*omega*t),[lv,1]); z=cat(3,z1,conj(z1));
```

```
for n=2:qd
 Dn=repmat(D(:,n,:),[1,M,1]);
 A=A1+Dn.*z.*A2; B=B1+Dn.*z.*B2; A2=A1; B2=B1; A1=A; B1=B;
end
ft=ft+A./B; ft=sum(ft,3)-repmat(Fs(:,1,2),[1,M,1]);
ft=repmat(exp(c*t)/NT,[lv,1]).*ft; ft(:,1)=2*ft(:,1);
switch depict
 case 'p1', plott1(t,ft); case 'p2', plott2(t,ft);
 case 'p3', plott3(t,ft); otherwise display('Invalid Plot');
end
```

```
% --- Plotting functions called by 1D NILT, vector version ----
%----------- Multiple plotting into single figure -------------
function plott1(t,ft)
figure; plot(t,real(ft)); grid on;
%figure; plot(t,imag(ft)); grid on; % optional
%----------- Plotting into separate figures ----------------
function plott2(t,ft)
for k=1:size(ft,1)
 figure; plot(t,real(ft(k,:))); grid on;
 figure; plot(t,imag(ft(k,:))); grid on; % optional
end
% ------------------ Plotting into 3D graphs ------------------
function plott3(t,ft)
global x; % x must be global in F
 m=length(t); tgr=[1:m/64:m,m]; % 65 time points chosen
 figure; mesh(t(tgr),x,real(ft(:,tgr)));
 figure; mesh(t(tgr),x,imag(ft(:,tgr)));
```

Code 5 (Exact solution with NILTcv)

```
clear
clc
R = 0;        % Resistance per unit length (Ohms per meter)
L = 2.5e-7;     % Inductance per unit length (Henries per meter)
G = 0;        % Conductance per unit length (Siemens per meter)
C = 1e-10;    % Capacitance per unit length (Farads per meter)
l = 400;    % Length of the transmission line (meters)
vs = 30;
t= 0:1e-11:20e-6;
h = t(2) - t(1);
% Calculate propagation constant (gamma) in the s-domain
z = @(s)(R+s.*L);
y = @(s)(G + s .* C);
gamma = @(s)sqrt(z(s) .* y(s));
% Calculate characteristic impedance (Z0) in the s-domain
Z0 = @(s) sqrt(z(s) ./ y(s));
% Calculate series impedance (Z_series) in the s-domain
Z_series =@(s) Z0(s) .* sinh(gamma(s) .* l);
Y_parallel =@(s) (1 ./ Z0(s)) .* tanh((gamma(s) .* l)./2); %y *tanh(gamma*l/2)
% Calculate parallel impedance (Z_parallel) in the s-domain
%Z_parallel =@(s) Z0(s) ./ tanh(gamma(s) .* l);
Z_parallel = @(s) 1./Y_parallel(s);
% Transfer function TF = Z_parallel / (Z_series + Z_parallel)
TF = @(s) Z_parallel(s) ./ (Z_series(s) + Z_parallel(s));
vo = @(s) TF(s) * vs./s;
```

```
%simplified
%vo = @(s) vs./(s.*cosh(l.*(G + C.*s).^(1/2).*(R + L.*s).^(1/2))); %
[y,t]=niltcv(vo,20e-6,'p1');
```

Code 6 (RLC to state space)

```
clear
clc
Rs =0;
Rdz = 5;
Ldz = 2;
Cdz =10;
N = 4;
numStates = 2 * N; % Each section has 2 states (current and voltage)
A = zeros(numStates, numStates);% Initialize A matrix
for i = 1:N
    if i == 1
        A(1, 1) = -(Rs + Rdz) / Ldz; % firs term (Rs + Rdz)
    else
        A(2*i-1, 2*i-1) = -Rdz / Ldz;
    end
    if i > 1
        A(2*i-1, 2*(i-1)) = 1 / Ldz;
        A(2*i-1, 2*i) = -1 / Ldz;
    end
    if i < N
        A(2*i-1, 2*i) = -1 / Ldz;
        A(2*i, 2*i-1) = 1 / Cdz;
        A(2*i, 2*i+1) = -1 / Cdz;
    else
        A(2*i, 2*i-1) = 1 / Cdz;
    end
end
% Initialize B matrix
B = zeros(numStates, 1);
B(1) = 1 / Ldz;
%C matrix
C = zeros(1, numStates);
C(end) = 1;
```

Code 7 (adapted FDTD for a lossy line)

```
function [y,t]=FDTD(R,L,C,length,Rs,t_max,N)
NDZ = N;  % Number of spatial steps
dz = length / NDZ;  % Spatial step delta z
dt = 1e-16;  % Time step delta t or Magic time step (dt = dz/v) for a lossles case
t_steps = round(t_max / dt);  % Number of time steps
% allocate voltage and current arrays
time = (0:t_steps-1)*dt;
V = zeros(NDZ+1, t_steps);
I = zeros(NDZ, t_steps);
f = 100e9;
% 1.Step input (1V source)
%Vs = 1 * ones(1, t_steps);
% 2. Sine wave (100 GHz)
Vs = sin(2*pi*f* time);
% 3. Trapezoidal pulse (custom function)
```

```
%for i=1:length(time)
    %Vs(i) = trapezoidalPulse(time(i));
%end
% FDTD Loop for Time Stepping
for n = 1:t_steps-1
     V(1, n+1) = (Rs*C/2*dz/dt+0.5)^-1*((Rs *C/2 *dz/dt-0.5)*V(1,n)-Rs*I(1,n)+0.5*(Vs(n+1)+Vs(n)));
    for k = 1:NDZ
    if k>1
        V(k,n+1) = V(k,n) + dt/(dz *C)* (I(k-1,n) - I(k,n));  % Update voltag
        I(k-1,n+1) = I(k-1,n)-(dt/(L*dz))*(V(k,n+1)-V(k-1,n+1))-(R*dt/L)*I(k-1,n);% Update current
    end
    end
    V(NDZ,n+1) =V(NDZ,n)+dt*(I(NDZ-1,n)/(C*dz));
end
y = V(NDZ,:);
t = time;
end
```

Code 8 (trapezoidal pulse function)

```
function v = trapezoidalPulse(t)
    % Define pulse parameters
    T_r = 1e-12;   % Rise time (1 ps)
    T_p = 5e-12;   % High-level duration (5 ps)
    T_total = 2*T_r + T_p;  % Total pulse duration (7 ps)

    % Piecewise definition of the pulse
    if t < 0
        v = 0;
    elseif t < T_r
        % Linear rise: from 0 to 1 V over T_r
        v = t / T_r;
    elseif t < T_r + T_p
        % Constant high level at 1 V
        v = 1;
    elseif t < T_total
        % Linear fall: from 1 V back to 0 over T_r
        v = (T_total - t) / T_r;
    else
        v = 0;
    end
end
```

Code 9 (AWE s=0)

```
function [h_impulse,h_s, y_step, t] = AWE(A,B,C,D,input,time)
    t = linspace(0,time,250);
    q = length(B);
    num_moments = 2 * q;
    moments = zeros(1, num_moments);
    [r,c]=size(C); % make sure C matrix in correct form
    if r~=1
        C= C';
    end
    for k = 1:num_moments
        moments(k) = (-1) * C * (A)^-(k) * B;
    end
    moments(1)=moments(1)+D;
    approx_order = length(B);
    % Construct the moment matrix
    moment_matrix = zeros(approx_order);
    Vector_c = -moments(approx_order+1:2*approx_order)';

    for i = 1:approx_order
        moment_matrix(i, :) = moments(i:i+approx_order-1);
    end

    % Solve for denominator coefficients
    b_matrix = moment_matrix^-1 * Vector_c;

    % Compute poles
    poles = roots([b_matrix', 1]);

    % Compute residues
    V = zeros(approx_order);
    for i = 1:approx_order
        for j = 1:approx_order
            V(i, j) = 1 / poles(j)^(i-1);
        end
    end

    A_diag = diag(1 ./ poles);
    r_moments = moments(1:approx_order);
    residues = -1 * (A_diag \ (V \ r_moments'));

    % Impulse response
    h_impulse = zeros(size(t));
    for i = 1:approx_order
        h_impulse = h_impulse + residues(i) * exp(poles(i) * t);
    end
    h_s =@(s) 0;
    for i = 1:length(poles)
        h_s =@(s) h_s(s) + residues(i)./(s-poles(i));
    end

    % Step response using recursive convolution
    y_step = zeros(size(t));
    y = zeros(length(poles), 1);

    for n = 2:length(t)
        dt = t(n) - t(n-1);
        exp_term = exp(poles * dt);
        for i = 1:length(poles)
            y(i) = residues(i) * (1 - exp_term(i))/(-poles(i)) * input + exp_term(i) * y(i);
        end
        y_step(n) = sum(y);
    end
end
```

Code 10 (generate Y parameters (rational approximation))

```
function [H_impulse,num,deno]=generate_yp2(realV,imagV,wo)
Yr = realV;  % Real part of Y11
Yi = imagV; % Imaginary part of Y11
w = wo;
A = [];
C = [];
% Loop through each frequency point to construct A and C
A = [];
```

```
C = [];
% Loop through each frequency point to construct A and C
for k = 1:length(w)
    wk = w(k);
    Yr_k = Yr(k);
    Yi_k = Yi(k);
    % Construct rows for A and C
    A_row1 = [-1, Yr_k, 0, -wk*Yi_k]; % Real part
    A_row2 = [0, Yi_k, -wk, wk*Yr_k]; % Imaginary part

    % Append to A
    A = [A; A_row1; A_row2];
    % C
    C_row1 = wk^2 * Yr_k; % Real part
    C_row2 = wk^2 * Yi_k; % Imaginary part
    % Append to C
    C = [C; C_row1; C_row2];
end

% Solve for B = [a0; b0; a1; b1]
B = A \ C;
% get cof
a0 = B(1);
b0 = B(2);
a1 = B(3);
b1 = B(4);
num = [a1,a0];
deno = [1,b1,b0];
% generated H
H_impulse =@(s) (a1*s+a0)./(s.^2+b1*s+b0);
end
```

Code 11 (Generate state space model)

```
function [A,B,C,D]= create_state_space(nem,deno)
N = nem;
D = deno;
% Perform polynomial division to make it strictly proper
[Q, R] = deconv(N, D);
% check leading coefficient (assumed to be 1)
if D(1) ~= 1
    D=D/D(1);
    N = N/D(1);
    [Q, R] = deconv(N, D);
end
% Extract coefficients for state-space representation
g = D(2:end);  % Exclude leading coefficient ( g terms )
% f terms
if R(1) ==0
    f=R(2:end);
else
    f = R;
end
% Construct state-space matrices
n = length(g); % Order of system
A = [zeros(n-1,1), eye(n-1); -flip(g)];
B = [zeros(n-1,1); 1];
C = flip(f);
D = Q;
end
```

Code 12 (AWE TL model)

```
clear
clc
% generate 100 points.
f = 1e6;
f = linspace(0,f,100);
w = 2*pi*f;
s = i *w;
% exact solution and generating 100 points
vo =1./(cosh(400.*(0 + 1e-10.*s).^(1/2).*(0.1 + 2.5e-7.*s).^(1/2)));
% to be used in NILT
v =@(s)1./(s.*cosh(400.*(0 + 1e-10.*s).^(1/2).*(0.1 + 2.5e-7.*s).^(1/2)));
first_idx = 1:6;
time = 50e-6;
models =23;
[~,num,deno] = generate_yp2(real(vo(first_idx)),imag(vo(first_idx)),w(first_idx));
R0 = num(end)/deno(end);
[A,B,C,D] = create_state_space(num,deno);
%HAWE is Hs= @(s) resdue/s-pole + ...;1 is the inout, 50e-6 is t for plot
[~,HAWEi, y0] = AWE2(A,B,C,D,w(1),1,time);
N =4; % number of points per section or model
range = 6; % starting point of the second mmodel
for i=1:models
    range = range(end):N + range(end); % raange of frequency and exact values
    H_diff = vo(range)-HAWEi(s(range));
    [~,numi,denoi] = generate_yp2(real(H_diff),imag(H_diff ),w(range));
    %numi=numi*R0;
    %numi(end)=numi(end)*R0;
    [A,B,C,D] = create_state_space(numi,denoi);
    R0 = numi(end)/denoi(end);
    [~,HAWEj, yi, ti] = AWE2(A,B,C,D,w(range(1)),1,time);
    HAWEi = @(s) HAWEi(s)+HAWEj(s);
    y0 = y0+yi;
end
[y1,t1]=niltcv(v,time,length(y0));
RMSE = sqrt(sum(abs(y0-y1).^2)/length(y1)); %unit step
RMSE2 = sqrt(sum(abs(HAWEi(s)-vo).^2)/length(vo));% impulse
figure
plot(t1,y1,ti,y0)
%plot(f,abs(vo),f,abs(HAWEi(s)))
grid on
xlabel('time s')
legend('AWE approximation', 'Exact');
title('approximation with models = ',num2str(models+1));
```